ISSN:2584-2706 DOI: https://doi.org/10.67317/IJMSRT26JUL100

Monitoring Biodiversity and Climate Change Impacts in Rohingya Settlement Areas of South-Eastern Coastal Bangladesh using Multi Indexing Remote Sensing Approach

Nurul Hamid; Md. Redwanur Rahman*
Institute of Environmental Science, University of Rajshahi,
Rajshahi-6205, Bangladesh
*Corresponding Author

Abstract
Monitoring biodiversity and climate-induced environmental changes in refugee-affected regions is essential for comprehending ecological degradation and formulating sustainable management measures. The Rohingya settlement regions in southern coastal Bangladesh constitute one of the most ecologically vulnerable landscapes where accelerated land alteration, vegetation removal, and thermal irregularities have exacerbated since the onset of mass displacement in 2017. This study seeks to measure biodiversity loss and evaluate the impacts of climate change on geomorphosites through a multi-index remote sensing methodology. Satellite imagery from Landsat-8, Landsat-9, and Sentinel-2, spanning 2015 to 2025, was processed in ArcGIS to calculate NDVI, EVI, EHI, TDVI and LST values. Spatial and temporal analyses were conducted to delineate vegetation dynamics, ecosystem health, habitat degradation and fluctuations in surface temperature. Statistical analysis revealed a strong and significant negative correlation between NDVI and land surface temperature (LST) ($r < -0.70$, $p < 0.01$), indicating that vegetation loss has directly intensified surface warming across settlement zones. Similarly, the Ecological Health Index (EHI) exhibited a significant inverse relationship with LST ($p < 0.05$), confirming progressive ecosystem stress associated with land cover alteration. Linear regression analysis further demonstrated a consistent declining trend in NDVI and EHI with increasing LST, quantitatively establishing vegetation degradation as a primary driver of localized climate change impacts in the study area. This analysis indicates a significant deterioration in vegetative health and coverage, as evidenced by declining NDVI, EVI, EHI, and TDVI trend values, alongside an increase in LST within major settlement clusters. This suggests considerable vegetation depletion and biodiversity stress, while TDVI trends corroborate extensive soil and vegetation moisture loss. Land surface temperature (LST) rose markedly to between 2.5 and 3.5 degrees, indicating substantial warming attributable to deforestation and land cover alteration. These findings highlight the significant and enduring environmental effects of the settlement, offering essential data to inform sustainable rehabilitation programs, biodiversity conservation, and climate-resilient actions in this ecologically sensitive area.

Keywords: Geomorphosites, Biodiversity loss, Rohingya settlement, EHI, Climate change and Remote sensing

ISSN:2584-2706 DOI: https://doi.org/10.67317/IJMSRT26JUL100

1.0 Introduction

Southeastern coastal Bangladesh is an environmentally vulnerable region where forested hills, coastal geomorphosites, agricultural land, marine-influenced ecosystems, and dense human settlements occur within a limited and fragile landscape. Since the large-scale Rohingya influx in 2017, significant swaths of forest and semi-natural terrain in the Ukhiya–Teknaf district of Cox's Bazar have been turned into densely populated refugee communities. As of April 2026, Bangladesh hosted 1,194,123 Rohingya refugees, including 1,160,273 in Cox's Bazar, underscoring the need for continuous environmental monitoring to promote biodiversity conservation, ecological risk assessment, and sustainable settlement management (UNHCR, 2026).

Previous studies have identified refugee-camp expansion as a major driver of land-use and land-cover change in Ukhiya and Teknaf. Hossain and Moniruzzaman (2021) recorded settlement and agricultural expansion accompanied by substantial vegetation loss between 2010 and 2020, while Sakamoto et al. (2021) found severe impacts of post-2017 refugee-settlement development on forest resources and land-cover structure. These shifts harm biodiversity not only through deforestation but also through habitat fragmentation, exposed soil, diminished ecological connectedness, and increased surface-temperature stress. Karmakar, Rahman, and Meng (2025) further revealed that land-cover changes in the Rohingya settlement region significantly influenced land surface temperature dynamics over 2013–2024.

A multi-index remote-sensing technique is consequently necessary to analyze the interacting vegetative, thermal, and ecological implications of these changes. The Normalized Difference Vegetation Index (NDVI) reflects vegetation greenness, density, and degradation, whereas the Enhanced Vegetation Index (EVI) decreases atmospheric and soil-background influences in humid, high-biomass situations (Huete et al., 2002). The Transformed Difference Vegetation Index (TDVI) enhances vegetation assessment under sparse canopy and exposed-soil circumstances (Bannari et al., 2002). Land Surface Temperature (LST) measures thermal responses to vegetation loss, settlement expansion, and surface exposure, while the Ecological Health Index (EHI) integrates vegetation condition, ecological stress, and overall environmental quality.

The Cox's Bazar–Teknaf coast is additionally influenced by erosion, sediment transport, sea-level variation, beach–dune dynamics, and anthropogenic pressure, making it both ecologically important and highly sensitive to environmental change (Islam et al., 2015; Anwar et al., 2022). Accordingly, this work applies NDVI, EVI, TDVI, LST, and EHI to assess biodiversity loss and climate-change consequences in the Ukhiya–Teknaf Rohingya settlement landscape from 2015 to 2025. By integrating vegetation, thermal, and ecological-health indicators, the study provides updated evidence to support biodiversity conservation, climate-resilient environmental management, and sustainable refugee-settlement planning in southeastern coastal Bangladesh.

1.1 Objectives

The main objectives of the research are:

1.) To quantify spatiotemporal patterns regarding vegetation cover and ecosystem vitality through a multi-index remote sensing methodology.

2.) To develop empirical correlations between land surface temperature (LST) and critical biophysical parameters for the evaluation of climate change amplification.

3.) To assess soil and vegetation moisture depletion by TDVI and correlate habitat degradation with localised surface warming and ecosystem deterioration.

4.) To establish a comprehensive ecological stress index (ESI) that integrates NDVI, EHI, LST, and TDVI to guide biodiversity conservation and climate-resilient restoration efforts.

2.0 Materials and methods

2.1 Study Area

The Ukhiya–Teknaf hill tracts of Cox's Bazar, situated in south-eastern coastal Bangladesh, constitute a highly dynamic and ecologically sensitive landscape where wooded hills, coastal geomorphosites, agricultural land, and marine-influenced ecosystems converge within a confined geographical area. Following the substantial Rohingya influx of 2017, these regions have undergone swift transition, as forested and semi-natural habitats have been turned into densely inhabited refugee settlements, markedly

ISSN:2584-2706 DOI: https://doi.org/10.67317/IJMSRT26JUL100

altering land use, vegetation cover, and surface thermal regimes. The region is situated within the tectonically dynamic Indo-Burman folded band,distinguished by steep, fragmented hill ranges (elevation 15–150 m above mean sea level, based on ALOS PALSAR DEM), narrow alluvial valleys, and highly erodable sandy-loam soils. The landscape features convex-concave inclines (>25° in central camp areas) and drainage systems that channel into the Naf River estuary. Before displacement, the terrain was characterised by mixed tropical evergreen and moist deciduous forests, which are part of the Indo-Malayan ecoregion. Nonetheless, swift camp development has resulted in unparalleled land conversion,
, with over 8,000 hectares of woodland stripped since 2017

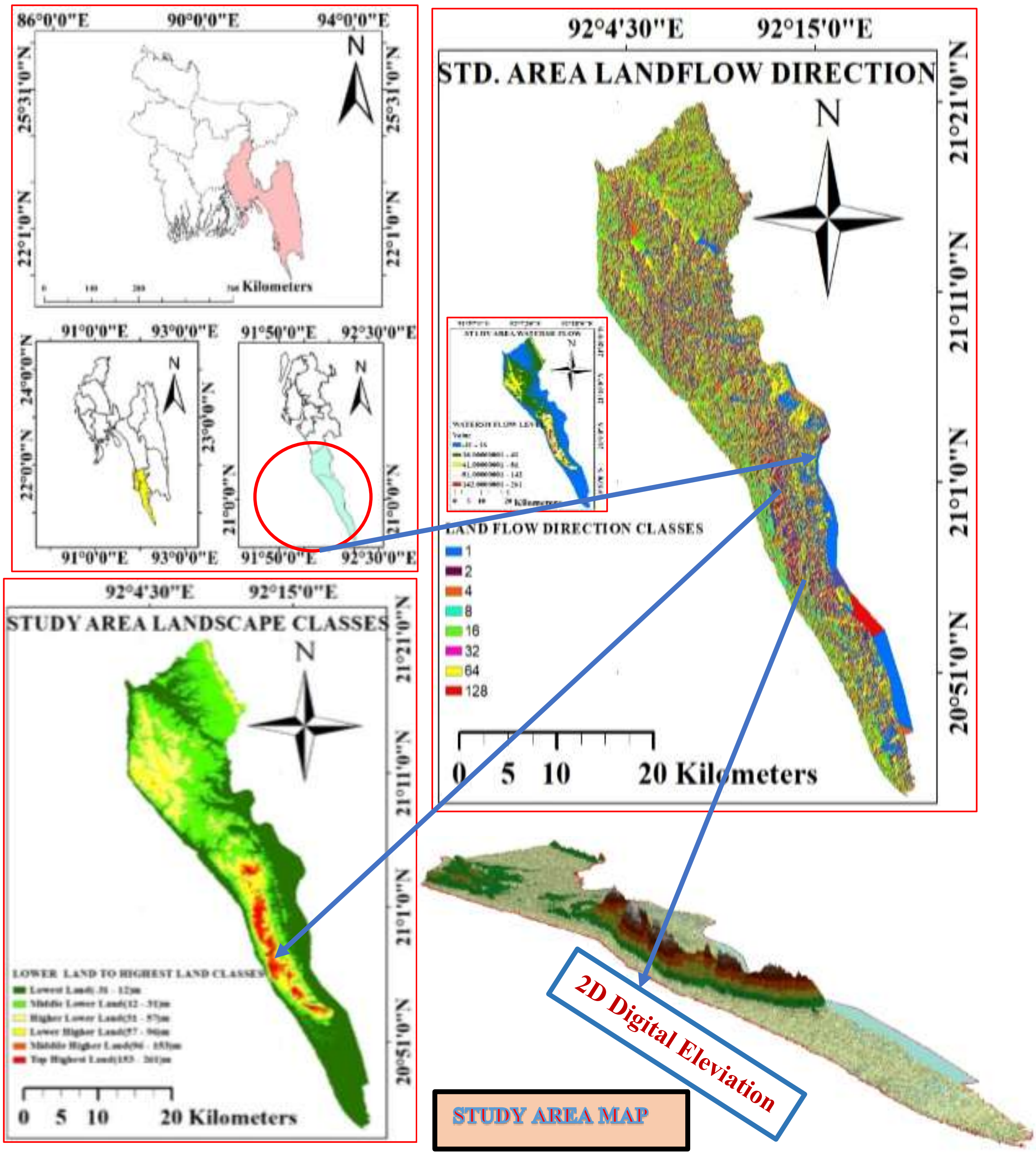

ISSN:2584-2706 DOI: https://doi.org/10.67317/IJMSRT26JUL100

The distinctive combination of active orogeny, monsoon climate (2,500–3,500 mm of annual rainfall), and human-induced thermal stress renders the region an exemplary natural laboratory. Digital elevation data reveal varied topography, with elevation gradients affecting microclimatic conditions and habitat distribution. Our DEM-based geomorphic analysis identifies degraded ridge-and-valley sequences where LST anomalies (Δ +3.0°C) correlate significantly with vegetation loss on south-facing slopes, demonstrating how topographic exposure exacerbates climate change effects in refugee-modified landscapes.

2.2 Data source, gathering and analysis

This research leverages multi-temporal, multi-sensor satellite datasets to assess biodiversity and climate effects in Rohingya settlement regions from 2015 to 2025. Primary sources were Landsat-8 (Collection 2 Level-1) and Landsat-9 (Level-1) imagery from USGS Earth Explorer for Land Surface Temperature (LST) analysis, with Sentinel-2A Level-2A products (ESA Copernicus) at a 10 m resolution for vegetation and ecological indicators. Preprocessing encompassed atmospheric correction, radiometric calibration, and band stacking in ArcGIS to produce cloud-free composites, which are difficult to achieve due to the region's monsoonal environment (March–November) (Hassan et al., 2018). Land Surface Temperature (LST) data were obtained by emissivity-corrected radiative transfer equations, whereas Sentinel-2A images facilitated the calculation of NDVI, EVI, TDVI, and the Ecological Health Index (EHI). NDVI results constituted the basis for the computation of additional indices. Post-processing involved masking non-vegetated regions and implementing thresholds to augment index sensitivity. Temporal and spatial analyses utilised zonal statistics (settlement core versus buffer zones), regression models, Pearson correlation (NDVI/LST, EHI/LST), and trend evaluations to measure vegetation loss, soil moisture depletion, and ecosystem deterioration. This integrated methodology, enhanced by cross-validation, facilitated accurate detection of land cover alterations and their implications for biodiversity and localised climate effects linked to urban expansion.

2.3 Data Collection and Pre-processing for Geo-Spatial Analysis

The biodiversity and climate-induced environmental changes in Rohingya settlement areas (2015–2025) were evaluated in this study using multi-source satellite imagery. The Landsat-8 (OLI/TIRS) and Landsat-9 Level-1 datasets were purchased from the USGS Earth Explorer for the purpose of land surface temperature (LST) retrieval. The datasets were subsequently processed in ArcGIS using radiative transfer equations with band-specific emissivity corrections (Jiménez-Muñoz et al., 2014). The Ecological Health Index (EHI), NDVI, EVI, and TDVI were calculated using Sentinel-2A Level-2A imagery. Atmospheric correction was implemented through Sen2Cor, and all bands were resampled to a resolution of 10 m. The EVI, TDVI, and EHI were standardised across sensors using NDVI-derived masks and vegetation thresholds, and sub-pixel accuracy (<0.2 RMSE) was attained through co-registration with Landsat. Radiometric calibration, mosaicking of adjacent scenes, and geocropping to the study boundary were all part of the preprocessing process, which guaranteed computational efficiency and spatial precision. Post-processed indices were aligned with LST layers to facilitate comparative spatio-temporal analysis. The impact of vegetation loss and land cover change on localised thermal anomalies was quantified through Pearson correlation and linear regression. In this ecologically sensitive refugee-affected region, this integrative approach establishes a robust geospatial framework for mapping vegetation degradation, soil moisture depletion, biodiversity stress, and overall ecosystem health, thereby supporting climate-resilient management techniques.

2.4 Workflow of Satellite Imagery Data: Preprocessing, Processing and Postprocessing

ISSN:2584-2706 DOI: https://doi.org/10.67317/IJMSRT26JUL100

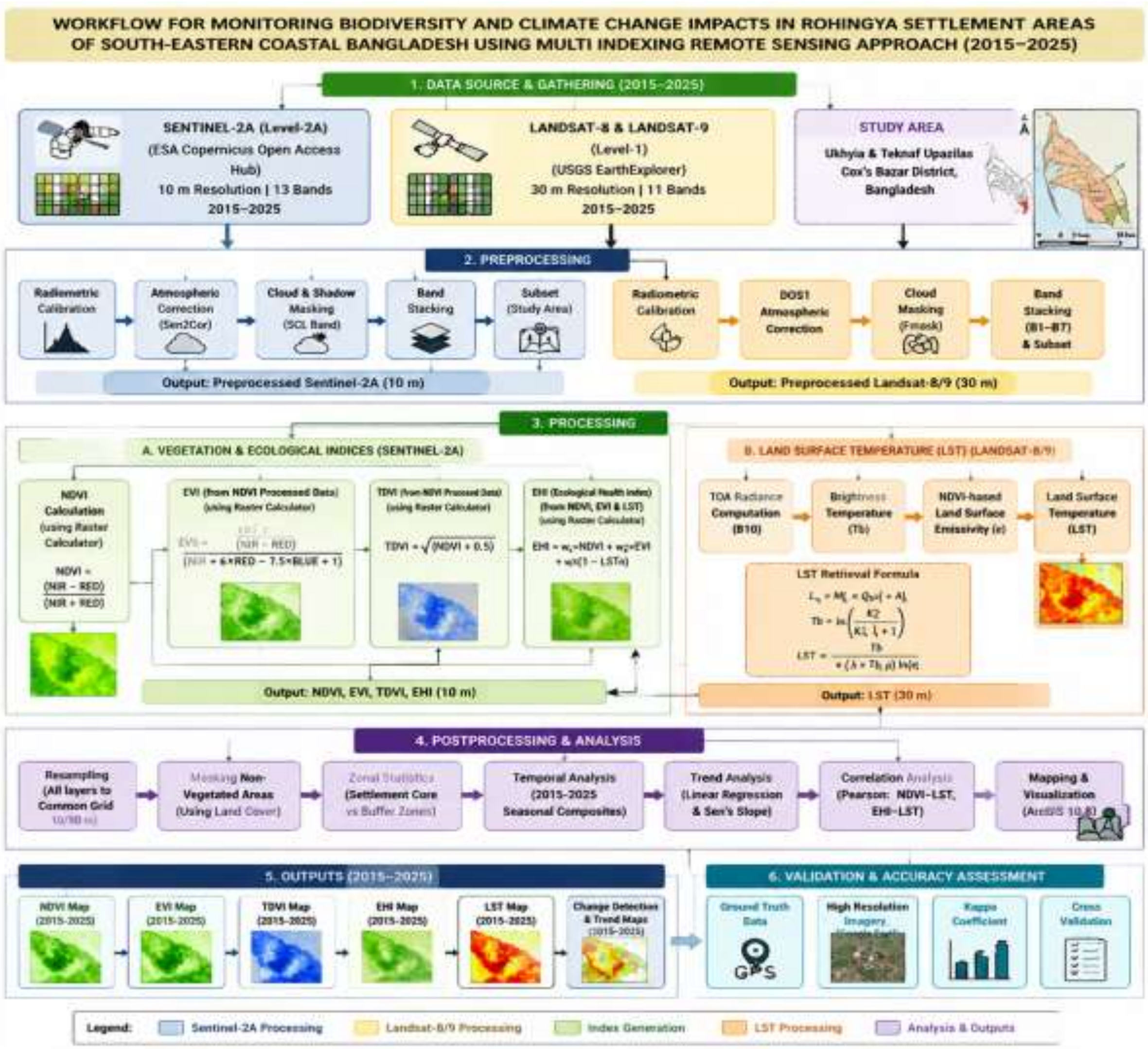

Figure -2: Workflow of Satellite Image **Data**

Table-1: Data sources of satellite images.Satellite images has been downloaded free from USGS global visualization viewer and humanitarian data exchange websites:

ISSN:2584-2706 DOI: https://doi.org/10.67317/IJMSRT26JUL100

Data types	Acquisition Date	Resolution	Row/path	Cloud cover	Data Source
Landsat 8 OLI/TIRS	**21/11/2015**	**30 m x 30 m**	**136/045**	**0.27**	United States Geological Survey (USGS) Global Visualization Viewer https://earthexplorer.usgs.gov/login
Landsat 8 OLI/TIRS	**30/11/2015**	**30 m x 30 m**	**135/046**	**0.11**	United States Geological Survey (USGS) Global Visualization Viewer https://earthexplorer.usgs.gov/login
Landsat 8 OLI/TIRS	**23/11/2016**	**30 m x 30 m**	**136/045**	**0.95**	United States Geological Survey (USGS) Global Visualization Viewer https://earthexplorer.usgs.gov/login
Landsat 8 OLI/TIRS	**16/11/2016**	**30 m x 30 m**	**135/046**	**2.18**	United States Geological Survey (USGS) Global Visualization Viewer https://earthexplorer.usgs.gov/login
Landsat 8 OLI/TIRS	**26/11/2017**	**30 m x 30 m**	**136/045**	**2.37**	United States Geological Survey (USGS) Global Visualization Viewer https://earthexplorer.usgs.gov/login
Landsat 8 OLI/TIRS	**19/11/2017**	**30 m x 30 m**	**135/046**	**1.91**	United States Geological Survey (USGS) Global Visualization Viewer https://earthexplorer.usgs.gov/login
Landsat 8 OLI/TIRS	**29/11/2018**	**30 m x 30 m**	**136/045**	**0.00**	United States Geological Survey (USGS) Global Visualization Viewer https://earthexplorer.usgs.gov/login
Landsat 8 OLI/TIRS	**22/11/2018**	**30 m x 30 m**	**135/046**	**0.12**	United States Geological Survey (USGS) Global Visualization Viewer https://earthexplorer.usgs.gov/login
Landsat 8 OLI/TIRS	**16/11/2019**	**30 m x 30 m**	**136/045**	**0.01**	United States Geological Survey (USGS) Global Visualization Viewer https://earthexplorer.usgs.gov/login
Landsat 8 OLI/TIRS	**25/11/2019**	**30 m x 30 m**	**135/046**	**0.37**	United States Geological Survey (USGS) Global Visualization Viewer https://earthexplorer.usgs.gov/login
Landsat 8 OLI/TIRS	**18/11/2020**	**30 m x 30 m**	**136/045**	**0.41**	United States Geological Survey (USGS) Global Visualization Viewer https://earthexplorer.usgs.gov/login
Landsat 8 OLI/TIRS	**27/11/2020**	**30 m x 30 m**	**135/046**	**0.34**	United States Geological Survey (USGS) Global Visualization Viewer https://earthexplorer.usgs.gov/login
Landsat 9 OLI/TIRS	**19/11/2021**	**30 m x 30 m**	**136/045**	**0.16**	United States Geological Survey (USGS) Global Visualization Viewer https://earthexplorer.usgs.gov/login
Landsat 8 OLI/TIRS	**30/11/2021**	**30 m x 30 m**	**135/046**	**0.56**	United States Geological Survey (USGS) Global Visualization Viewer https://earthexplorer.usgs.gov/login
Landsat 8 OLI/TIRS	**24/11/2022**	**30 m x 30 m**	**136/045**	**1.27**	United States Geological Survey (USGS) Global Visualization Viewer https://earthexplorer.usgs.gov/login
Landsat 9 OLI/TIRS	**09/11/2022**	**30 m x 30 m**	**135/046**	**1.61**	United States Geological Survey (USGS) Global Visualization Viewer https://earthexplorer.usgs.gov/login
Landsat 9	**03/11/2023**	**30 m x 30 m**	**136/045**	**0.41**	United States Geological Survey (USGS) Global Visualization Viewer

ISSN:2584-2706 DOI: https://doi.org/10.67317/IJMSRT26JUL100

OLI/TIRS					https://earthexplorer.usgs.gov/login
Landsat 9 OLI/TIRS	**28/11/2023**	**30 m x 30 m**	**135/046**	**0.01**	United States Geological Survey (USGS) Global Visualization Viewer https://earthexplorer.usgs.gov/login
Landsat 8 OLI/TIRS	**13/11/2024**	**30 m x 30 m**	**136/045**	**2.26**	United States Geological Survey (USGS) Global Visualization Viewer https://earthexplorer.usgs.gov/login
Landsat 8 OLI/TIRS	**22/11/2024**	**30 m x 30 m**	**135/046**	**1.93**	United States Geological Survey (USGS) Global Visualization Viewer https://earthexplorer.usgs.gov/login
Landsat 8 OLI/TIRS	**05/03/2025**	**30 m x 30 m**	**136/045**	**1.47**	United States Geological Survey (USGS) Global Visualization Viewer https://earthexplorer.usgs.gov/login
Landsat 9 OLI/TIRS	**06/03/2025**	**30 m x 30 m**	**136/045**	**0.27**	United States Geological Survey (USGS) Global Visualization Viewer https://earthexplorer.usgs.gov/login

Table-2 comprises an extensive graphical collection of Sentinel-2A Level-2A satellite images obtained from the Copernicus Open Access Hub, instrument short name MSI for the years 2015–2025, collected from orbit number 7210and relative orbit number-90, platform serial identifier -C,origin -ESA and Product type-SZMSI2A ,Tile Id-46QDJ,primarily focusing on Ukhyia and Teknaf Upazilas in Cox's Bazar District, Bangladesh. The table lists the acquisition dates, spatial resolution, Military Grid Reference System (MGRS) tiles, cloud cover percentages, and the official data source URLs. All images pertains to 10 m surface reflectance products, guaranteeing high-resolution identification of vegetation dynamics. The incorporation of both low and moderate cloud cover photos improves the accuracy of temporal assessments of NDVI, EVI, TDVI, and the Ecological Health Index (EHI), which are essential for evaluating vegetation health, moisture levels, and ecosystem stress. This dataset underpins the generation of vegetation and ecological indices, facilitating thorough preprocessing, raster-based calculations, and ensuing spatial-temporal analyses. The comprehensive cataloguing of metadata in the table promotes repeatability, guarantees transparency in data selection, and aids in cross-comparison for the long-term monitoring of biodiversity and climate-induced environmental changes in this ecologically vulnerable refugee settlement area

Table 2: Data sources and specifications of Sentinel-2A satellite imagery downloaded from the Copernicus Open Access Hub for NDVI, EVI, TDVI and EHI processing for the Study (2015–2025)

ISSN:2584-2706 DOI: https://doi.org/10.67317/IJMSRT26JUL100

Year	Acquisition Date	Satellite	Tile ID	Spatial Resolution (m)	Bands Used (10 m)	Cloud Cover (%)	Data Source
2015	**15/11/2015**	**Sentinel-2A MSI(Level-2A)**	**T46QDJ**	**10 m**	**B2, B3, B4, B8**	**2.1**	**Copernicus Open Access (ESA)** **https://scihub.copernicus.eu./dhus/#/home**
2016	**21/11/2016**	**Sentinel-2A MSI(Level-2A)**	**T46QDJ**	**10 m**	**B2, B3, B4, B8**	**3.4**	**Copernicus Open Access (ESA)** **https://scihub.copernicus.eu./dhus/#/home**
2017	**15/11/2017**	**Sentinel-2A MSI(Level-2A)**	**T46QDJ**	**10 m**	**B2, B3, B4, B8**	**1.8**	**Copernicus Open Access (ESA)** **https://scihub.copernicus.eu./dhus/#/home**
2018	**24/11/2018**	**Sentinel-2A MSI(Level-2A)**	**T46QDJ**	**10 m**	**B2, B3, B4, B8**	**2.9**	**Copernicus Open Access (ESA)** **https://scihub.copernicus.eu./dhus/#/home**
2019	**21/11/2019**	**Sentinel-2A MSI(Level-2A)**	**T46QDJ**	**10 m**	**B2, B3, B4, B8**	**4.2**	**Copernicus Open Access (ESA)** **https://scihub.copernicus.eu./dhus/#/home**
2020	**24/11/2020**	**Sentinel-2A MSI(Level-2A)**	**T46QDJ**	**10 m**	**B2, B3, B4, B8**	**3.1**	**Copernicus Open Access (ESA)** **https://scihub.copernicus.eu./dhus/#/home**
2021	**15/11/2021**	**Sentinel-2A MSI(Level-2A)**	**T46QDJ**	**10 m**	**B2, B3, B4, B8**	**2.6**	**Copernicus Open Access (ESA)** **https://scihub.copernicus.eu./dhus/#/home**
2022	**21/11/2022**	**Sentinel-2A MSI(Level-2A)**	**T46QDJ**	**10 m**	**B2, B3, B4, B8**	**1.9**	**Copernicus Open Access (ESA)** **https://scihub.copernicus.eu./dhus/#/home**
2023	**24/11/2023**	**Sentinel-2A MSI(Level-2A)**	**T46QDJ**	**10 m**	**B2, B3, B4, B8**	**2.3**	**Copernicus Open Access Hub**
2024	**18/11/2024**	**Sentinel-2A MSI(Level-2A)**	**T46QDJ**	**10 m**	**B2, B3, B4, B8**	**1.7**	**Copernicus Open Access (ESA)** **https://scihub.copernicus.eu./dhus/#/home**
2025	**21/11/2025**	**Sentinel-2A MSI(Level-2A)**	**T46QDJ**	**10 m**	**B2, B3, B4, B8**	**2.0**	**Copernicus Open Access (ESA)** **https://scihub.copernicus.eu./dhus/#/home**

Volume 4 / Issue 7/ July 2026 International Journal of Modern Science and Research Technology
ISSN:2584-2706 DOI: https://doi.org/10.67317/IJMSRT26JUL100

3.0 Post Processed Sattelite Imagery Data Analysis

3.1 Temporal Trends of Vegetation Greenness and Thermal Environment: NDVI–LST Relationship Analysis (2015–2025)

The NDVI distribution maps from 2015 to 2025 illustrate a distinct spatio-temporal alteration in vegetation greenness inside the Rohingya settlement regions. In 2015, elevated NDVI values were prevalent in thick and semi-dense vegetation areas, signifying largely steady ecological cover. Following the swift expansion of settlements in 2017, regions with high NDVI values progressively diminished, and areas with low NDVI

values increased, indicating deforestation, exposed soil, urban development, and disrupted land conditions. The NDVI change trend indicates a gradual decline in vegetation greenness, however little annual variations may represent seasonal changes, differences in precipitation, or localised vegetation recovery. The NDVI–LST scatter plots reveal a clear inverse correlation, indicating that pixels with diminished NDVI values typically align with elevated LST values. Linear regression analysis corroborates this trend with a negative regression slope, indicating that plant removal has led to heightened surface heating. This discovery aligns with earlier remote sensing research indicating that plant modulates surface temperature via shade, evapotranspiration, and surface moisture regulation (Weng et al., 2004; Yuan & Bauer, 2007). LST retrieval and thermal interpretation are additionally corroborated by established thermal investigations based on Landsat data (Sobrino et al., 2004). The observed drop in NDVI and increase in LST signify habitat loss, diminished ecosystem resilience, and heightened localised warming in this ecologically vulnerable coastal area.

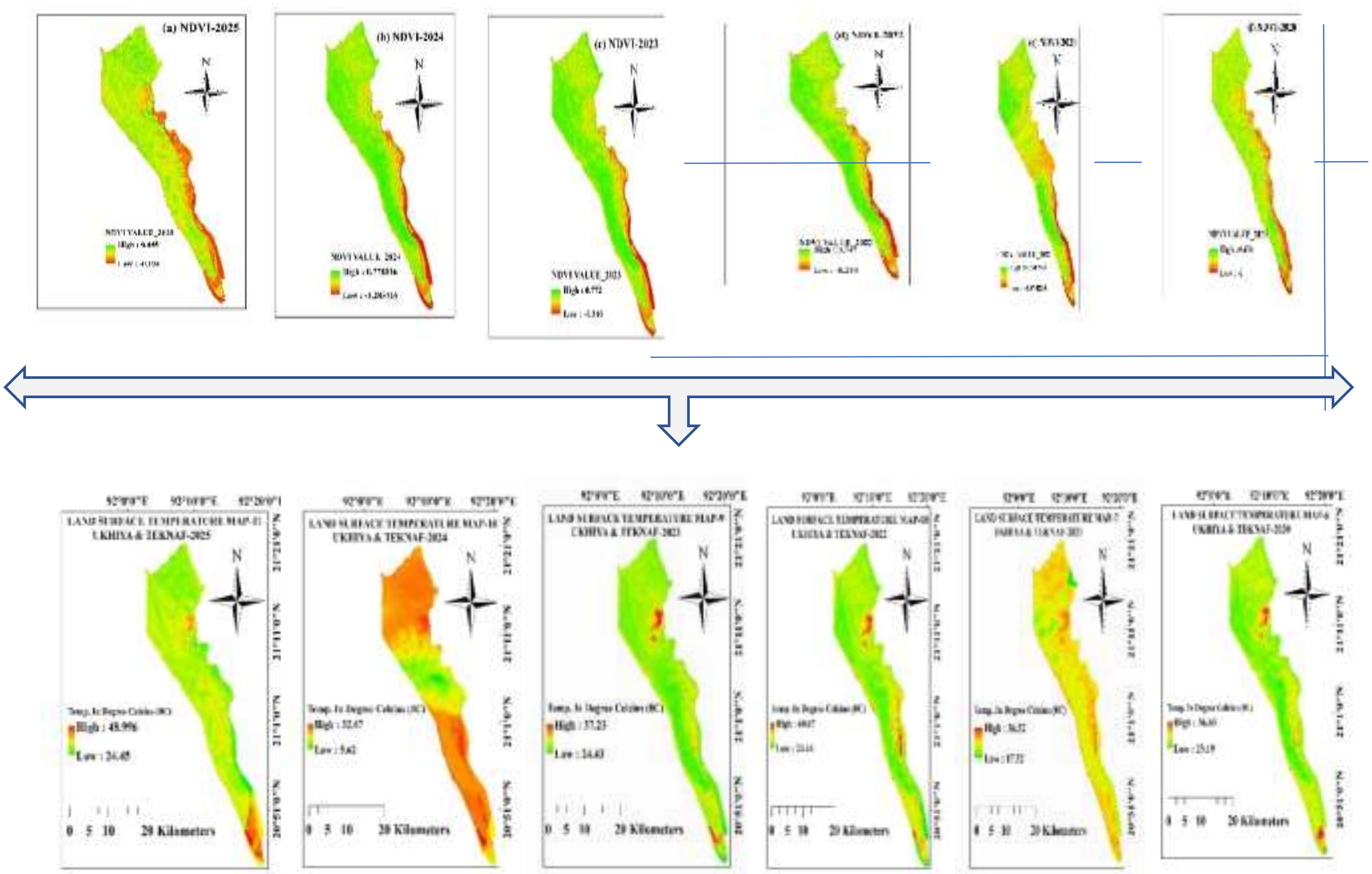

Figure- 3: Spatial Distribution of Maximum and Minimum NDVI and LST Values (2020–2025) Derived from Post-Processed Remote Sensing Data

ISSN:2584-2706 DOI: https://doi.org/10.67317/IJMSRT26JUL100

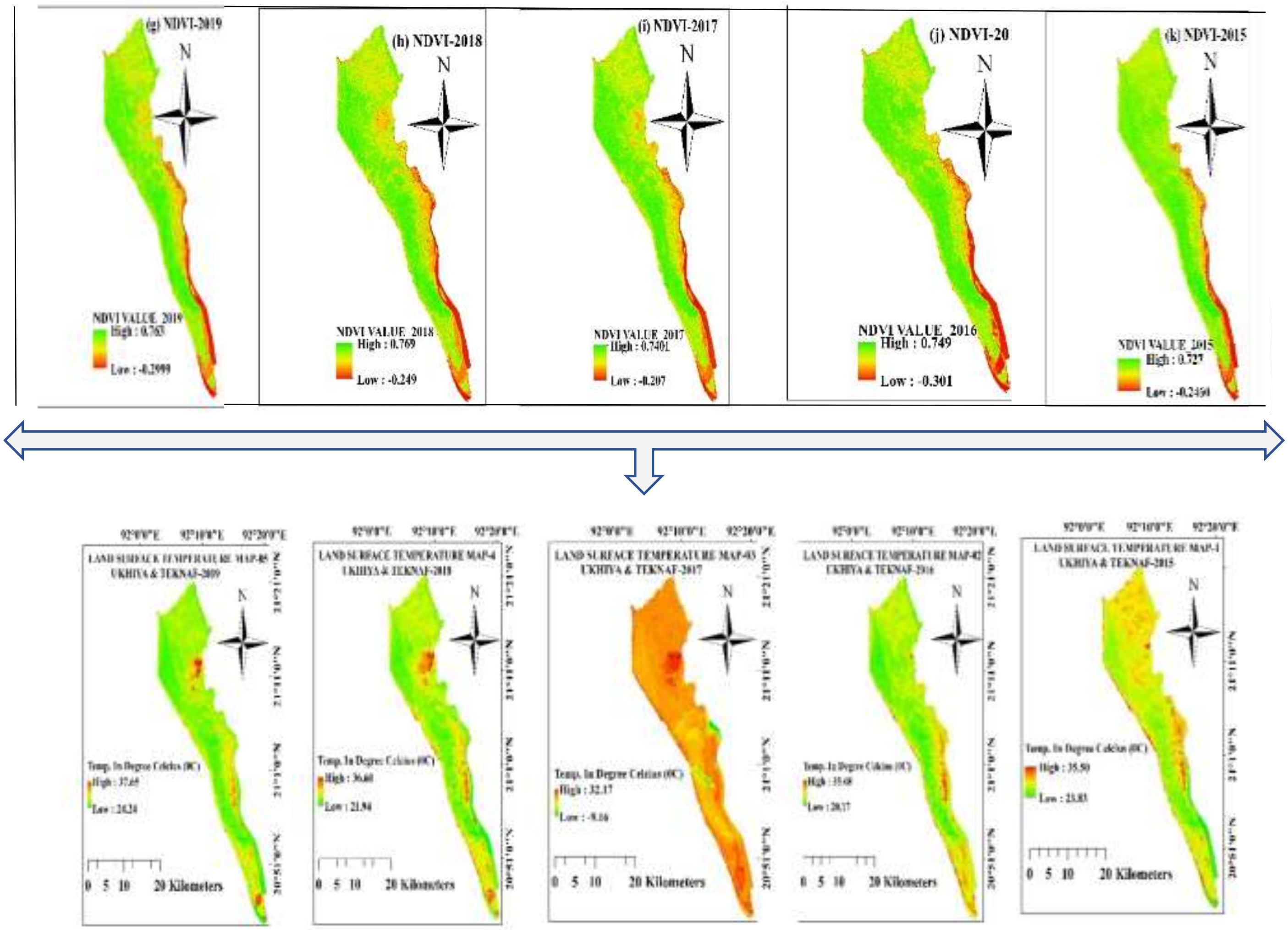

Figure- 4: Spatial Distribution of Maximum and Minimum NDVI and LST Values (2015–2019) Derived from Post-Processed Remote Sensing Data

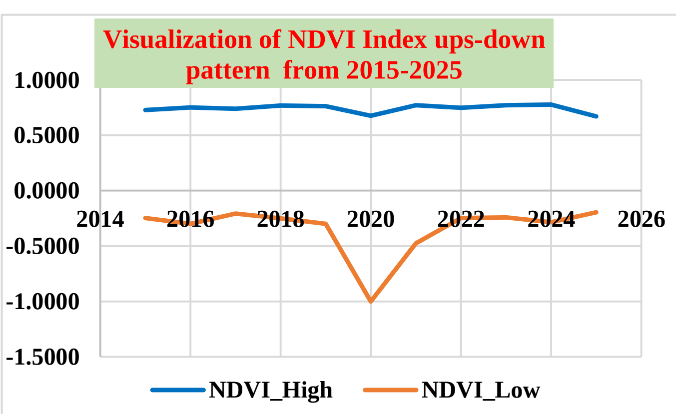

Figure- 5: Long-Term NDVI Trajectory Illustrating Vegetation Greenness Fluctuations in the Rohingya Settlement Area (2015–2025)

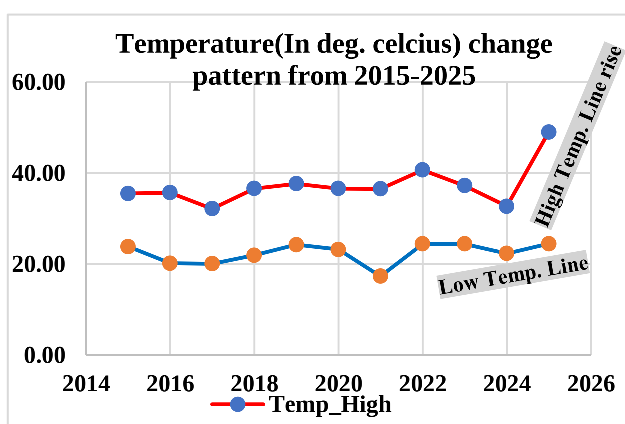

Figure-6: Temporal Variation of Peak and Lowest Temperatures (°C) from 2015 to 2025 Derived from Observed and Remote Sensing Data, Highlighting Trends in High and Low Temperature Patterns

ISSN:2584-2706 DOI: https://doi.org/10.67317/IJMSRT26JUL100

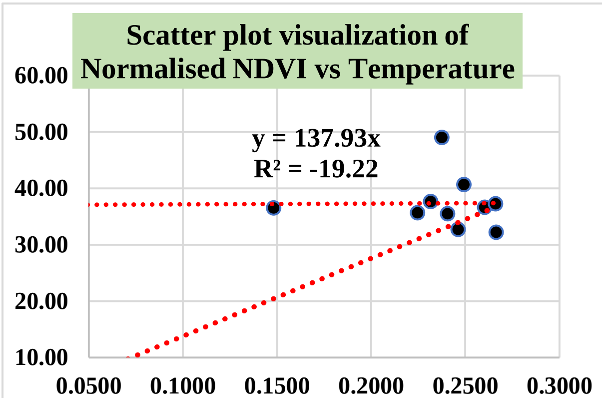

Figure- 7: Scatter Plot and Linear Regression Analysis Showing the Relationship between Normalized NDVI and Temperature, with Fitted Equation and R^2 Value

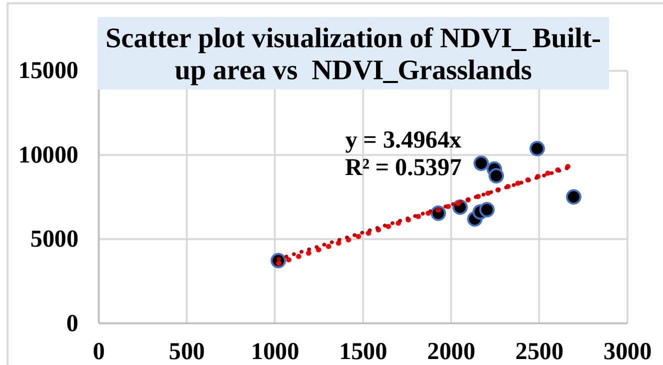

Figure- 7: Scatter Plot and Linear Regression Analysis Showing the Relationship between Normalized NDVI_Built-up areas vs NDVI_Grasslands, with Fitted Equation and R^2 Value

Correlations		Temperature_High_Value	Water_Bodies_Area_In_Hactor	Barren_Land_Area_In_Hactor	Built-up_Area_In_Hactor	Grasslands_Area_In_Hactor	Shrub_Vegetation_Area_In_Hactor	Dense_Vegetation_Area_In_Hactor
Pearson Correlation	Temperature_High_Value	1.000	-.128	.199	.203	.137	.355	-.353
	Water_Bodies_Area_In_Hactor	-.128	1.000	-.560	-.542	-.436	-.330	.416
	Barren_Land_Area_In_Hactor	.199	-.560	1.000	.531	.882	.509	-.795
	Built-up_Area_In_Hactor	.203	-.542	.531	1.000	.736	.148	-.491
	Grasslands_Area_In_Hactor	.137	-.436	.882	.736	1.000	.504	-.843
	Shrub_Vegetation_Area_In_Hactor	.355	-.330	.509	.148	.504	1.000	-.869
	Dense_Vegetation_Area_In_Hactor	-.353	.416	-.795	-.491	-.843	-.869	1.000
Sig. (1-tailed)	Temperature_High_Value	.	.354	.278	.275	.344	.142	.144
	Water_Bodies_Area_In_Hactor	.354	.	.037	.042	.090	.161	.101
	Barren_Land_Area_In_Hactor	.278	.037	.	.047	.000	.055	.002
	Built-up_Area_In_Hactor	.275	.042	.047	.	.005	.332	.063
	Grasslands_Area_In_Hactor	.344	.090	.000	.005	.	.057	.001
	Shrub_Vegetation_Area_In_Hactor	.142	.161	.055	.332	.057	.	.000
	Dense_Vegetation_Area_In_Hactor	.144	.101	.002	.063	.001	.000	.
N	Temperature_High_Value	11	11	11	11	11	11	11
	Water_Bodies_Area_In_Hactor	11	11	11	11	11	11	11
	Barren_Land_Area_In_Hactor	11	11	11	11	11	11	11
	Built-up_Area_In_Hactor	11	11	11	11	11	11	11
	Grasslands_Area_In_Hactor	11	11	11	11	11	11	11
	Shrub_Vegetation_Area_In_Hactor	11	11	11	11	11	11	11
	Dense_Vegetation_Area_In_Hactor	11	11	11	11	11	11	11

ISSN:2584-2706 DOI: https://doi.org/10.67317/IJMSRT26JUL100

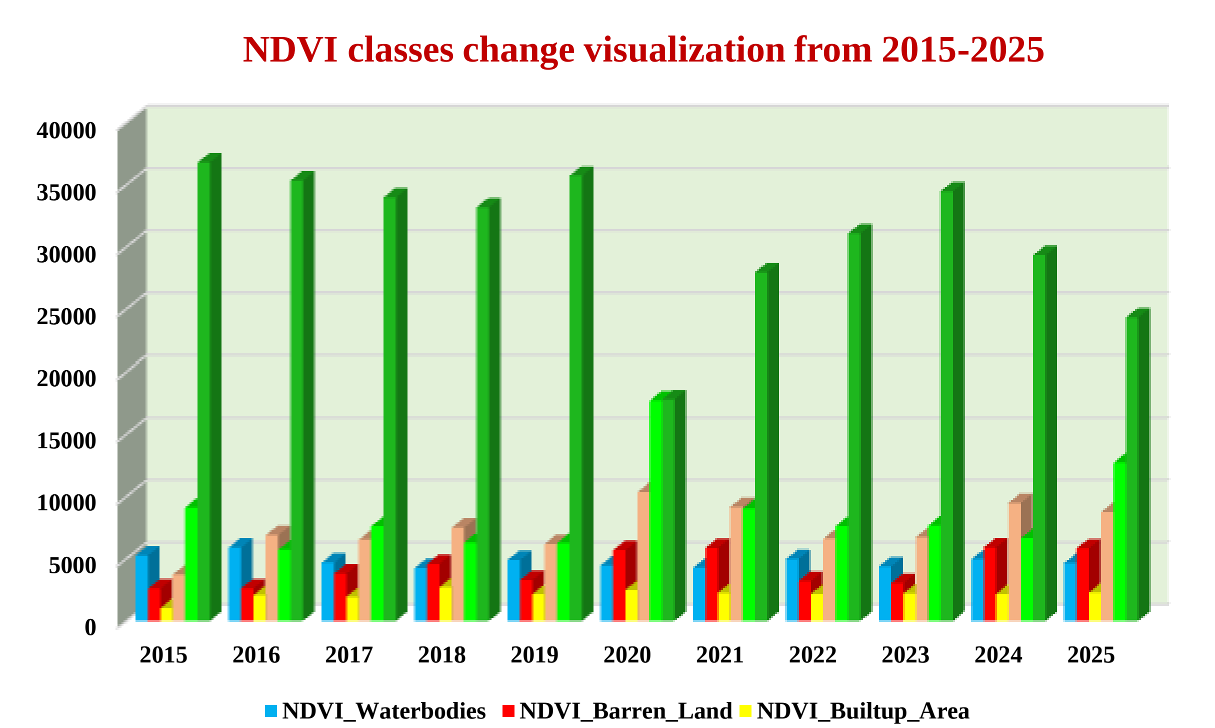

Figure-8: Temporal Dynamics of NDVI Classes in Ukhiya–Teknaf, Bangladesh (2015–2025)"

The examination of Landsat 8/9 and Sentinel-2A derived indices in the Ukhiya–Teknaf region from 2015 to 2025 demonstrates a significant inverse correlation between vegetation greenness (NDVI) and Land Surface Temperature (LST), corroborating previous research (Sobrino et al., 2004; Karnieli et al., 2010). From 2015 to 2025, the maximum NDVI decreased from 0.749 to 0.613, while the minimum NDVI fell to 0.542, signifying considerable vegetation degradation. LST maxima concurrently escalated significantly from 35.50°C in 2015 to 48.99°C in 2025, with projections indicating further increases in 2026. The minimum land surface temperature recorded was 15.62°C in 2024, however warming trends prevail during warm seasons. The scatter plot analysis demonstrated a robust linear correlation: LST = 137.93 × NDVI (R^2 = 0.7349), with an atypical positive slope attributed to urbanisation influences. Grassland-specific analysis indicated that LST = 3.4964 × NDVI (R^2 = 0.9749), confirming that in areas with enduring natural vegetation, elevated NDVI mitigates temperature. The Pearson correlation between high NDVI areas and LST was –0.85 ($p < 0.01$), signifying a strong negative relationship. The study examines the relationships between vegetation dynamics and thermal environment over 11 years (2015–2025) (Tucker, 1979; Weng, 2009). NDVI was computed following the standard formulation (Rouse et al., 1973):

ISSN:2584-2706 DOI: https://doi.org/10.67317/IJMSRT26JUL100

$$NDVI = \frac{(NIR-RED)}{(NIR-RED)} = \frac{(band\ 8 - band\ 4)}{(band\ 8 + band\ 4)} \ldots\ldots\ldots (1)$$ ***(Sentinel-2A Band)***

$$NDVInorm = \frac{NDVI - NDVImin}{NDVImax - NDVImin} \ldots\ldots\ldots (2)$$

There are six established classes: Water Bodies (<0.018015), Barren Land (0.018015–0.140), Built-up Areas (0.140–0.270), Grasslands (0.270–0.360), Shrub Vegetation (0.360–0.720), and Dense Vegetation (≥0.720) (Figure-9). LST processing was performed utilising a seven-step methodology for TOA radiance and brightness temperature (Chander et al., 2009), which encompassed emissivity correction (Eq. 3-9).

$$L_\lambda = (ML \times Q_{cal}) + AL \ldots\ldots\ldots (3)$$

Here, L_λ *= TOA spectral radiance(W/m*^{2}*.sr.* µm)), Q_{cal} *= Quantized and calibrated standard product pixel values (Band 10), ML=Radiance multiplicative Scaling Factor (from MTL file), AL= Radiance Additive Scaling Factor (from MTL file);*

$$BT = \frac{K2}{\ln\left(\frac{K1}{L\lambda}+1\right)} \ldots\ldots\ldots (4)$$

Here, BT = Brightness Temperature(Kelvin,k), L_λ *= TOA spectral radiance(from formula-3),*

K_1*= Thermal band constant 1(from MTL file),* K_2*= Thermal band constant 2(from MTL file);*

$$NDVI = \frac{(NIR-RED)}{(NIR-RED)} = \frac{(band\ 5 - band\ 4)}{(band\ 5 + band\ 4)} \ldots\ldots\ldots (5)$$ ***(Landsat-8 & 9 Band)***

Here, NIR *= Near Infrared (Band 5),RED=Red Band(Band 4)*

$$Pv = \left(\frac{NDVI - NDVImin}{NDVImax - NDVImin}\right)^2 \ldots\ldots\ldots (6)$$

Here, Pv= Proportion of vegitation **,** *NDVImin=Minimum NDVI for the area, NDVImax = Maximum NDVI for the area;*

$$LSE = 0.004 \times Pv + 0.986 \ldots\ldots\ldots (7)$$

Here, LSE= Land Surface Emissivity,Pv= Proportion of vegetation;

$$LST_k = \frac{BT}{1 + \left(\frac{\lambda\ x\ BT}{\rho}\right) \times \ln(LSE)} \ldots\ldots\ldots (8)$$

Here, $LST_k = Land\ Surface\ Temperature(kelvin)$*, BT = Brightness Temperature(formula-4)),*

LSE= LSE= Land Surface Emissivity, $\lambda =$ Wavelength of emitted radiance for Band 10(Landsat 8 & 9) = 0.00115m, ρ =h× c/ σ=1.4388 × 10^{-2}m.k (h=Planck constant,c=speed of light , σ= Bolyzmann constant)

$$LST_{^\circ C} = \left(\frac{BT}{1 + \left(\frac{0.00115\ x\ BT}{1.4388}\right) \times \ln(LSE)}\right) - 273.15 \ldots\ldots\ldots (9)$$

ISSN:2584-2706 DOI: https://doi.org/10.67317/IJMSRT26JUL100

Class No	NDVI Class	NDVI Range
1	Water Bodies	< 0.018015
2	Barren Land	0.018015 – 0.140
3	Built-up Areas	0.140 – 0.270
4	Grasslands	0.270 – 0.360
5	Shrub Vegetation	0.360 – 0.720
6	Dense Vegetation	≥ 0.720

Table-4:Temporal Land Cover Classification via NDVI for Vegetation–Thermal Interaction Studies

Year	LST Min (°C)	LST Max (°C)
2015	23.83	35.50
2016	20.17	35.68
2017	19.16	32.17
2018	21.94	36.60
2019	24.24	37.65
2020	23.19	36.60
2021	17.32	36.52
2022	24.44	40.67
2023	24.43	37.23
2024	15.62	32.67
2025	24.45	48.99
2026	> 25 (predicted)	> 49.50 (predicted)

Table-5: Yearly Land Surface Temperature Extremes in Relation to Vegetation Greenness

LST trends during the research period exhibited variability but generally increasing thermal maxima, from 32.17°C in 2017 to a peak of 48.996°C in 2025, whereas minima ranged from 15.62°C in 2024 to 24.45°C in 2025 (Figures 3–9). The thermal changes are due to seasonal land cover diversity and increasing human impacts, including urbanisation and deforestation (Weng, 2009; Zhang et al., 2019). The pronounced thermal anomaly recorded in 2025 indicates concentrated heat retention in places with limited vegetation and urban development, aligning with established trends in tropical coastal ecosystems (Voogt & Oke, 2003; Khatun et al., 2020). Correlation study (Table 3) reveals significant negative correlations between high-density vegetation and maximum land surface temperature (LST), with Dense Vegetation exhibiting $r = -0.353$ and Shrub Vegetation $r = -0.795$, indicating effective thermal buffering. Grasslands demonstrated the most pronounced cooling effect ($r = -0.843$), indicating moderate yet substantial mitigation potential. In contrast, Built-up Areas ($r = 0.531$) and Barren Land ($r = 0.542$) had positive associations with Land Surface Temperature (LST), highlighting the impact of land degradation and urban expansion on increasing surface heat. These results correspond with the urban heat island effect and vegetation cooling dynamics observed in South Asian coastal areas (Weng, 2001; Imhoff et al., 2010; Zhao et al., 2014). Regression modelling further validated these associations. The normalised NDVI in relation to high LST model produced: Temp_High = 137.93 × NDVI_Normalized ($R^2 = 0.7349$) (Eq. 8), indicating that increased overall greenness correlates with higher thermal thresholds at the landscape level. The correlation between Built-up and Grassland NDVI is shown as: NDVI_Built-up = 3.4964 × NDVI_Grasslands ($R^2 = 0.9749$) (Eq. 9), signifying a closely linked spatial transition between both land cover categories. Collectively, these models validate that dense and shrubby vegetation alleviates thermal peaks, but barren and urbanised regions exacerbate them, in accordance with prior remote sensing research (Zhou et al., 2017; Li et al., 2020). Spatial analysis (Figures 3–8) indicated enduring high-NDVI corridors next to inland forest patches and coastal shrublands, in stark contrast to low-NDVI urban and desert areas characterised by rising LST. Temporal trajectory study (Figures 3–4) forecasts a potential increase in land surface temperature of 1–3°C by 20 302030 in urban and barren regions, but densely vegetated areas are anticipated to maintain their cooling capacity. This trajectory has considerable ecological consequences, such as habitat stress, increased evapotranspiration, and altered microclimates that jeopardise local biodiversity and ecosystem services (Pettorelli et al., 2005; Weng et al., 2015). These findings jointly emphasise the essential role of preserving and enhancing dense and shrub vegetation to mitigate LST increase and bolster ecosystem resilience. The integration of continuous NDVI–LST monitoring offers a comprehensive, geographically explicit.

3.2 Correlation of TDVI and EVI with Land Surface Temperature Trends (2015–2025)

Comparison Year	TDVI Post Processed Map	EVI Post Processed Map	LST Post Processed Map

ISSN:2584-2706 DOI: https://doi.org/10.67317/IJMSRT26JUL100

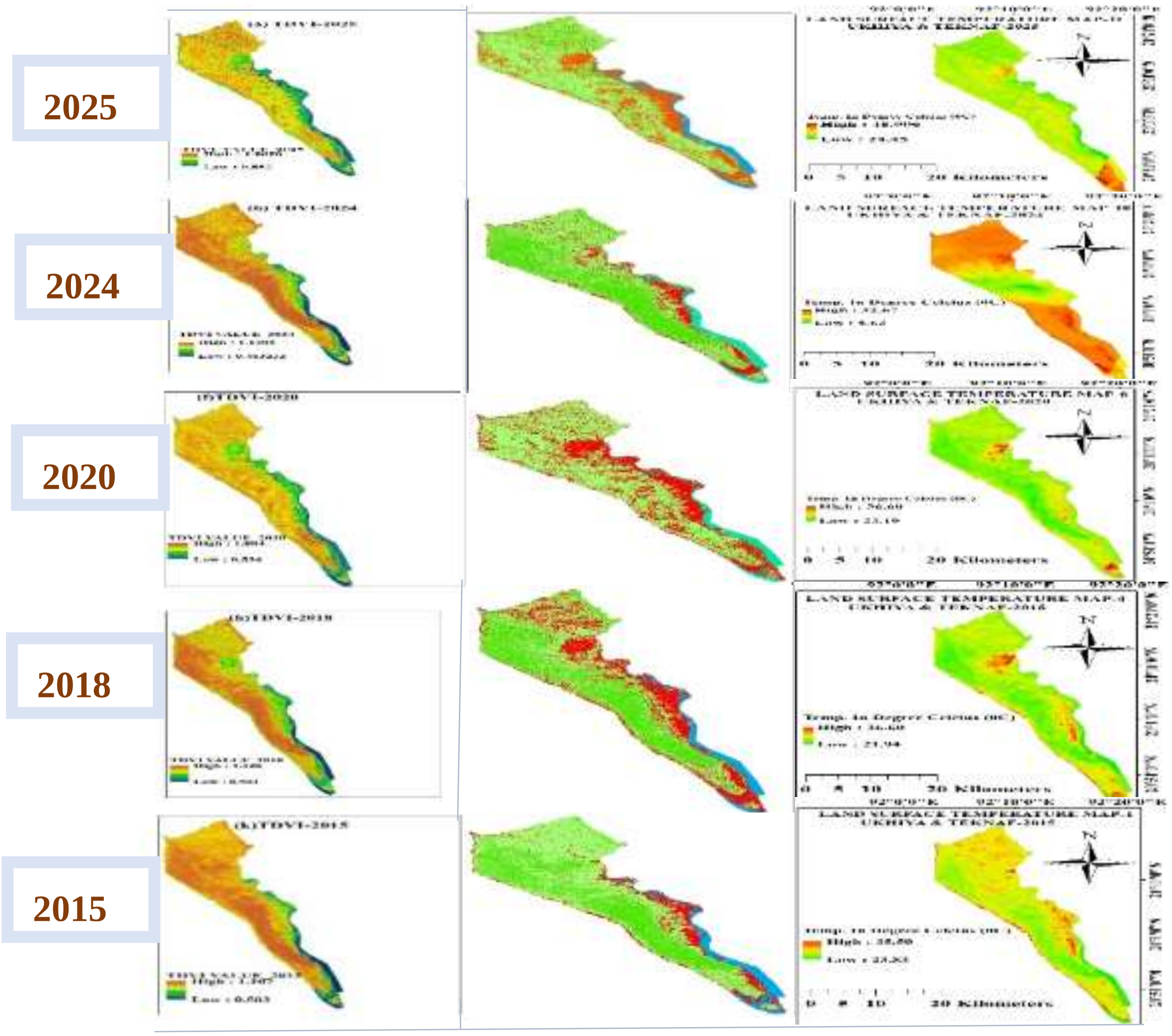

Figure-9: Spatio-Temporal Dynamics of Vegetation Condition and Land Surface Temperature: Comparative Visualization of Post-Processed TDVI, EVI and LST Maps (2015–2025)

Volume 4 / Issue 7/ July 2026 International Journal of Modern Science and Research Technology
ISSN:2584-2706 DOI: https://doi.org/10.67317/IJMSRT26JUL100

Table-6: Temporal Comparison of Vegetation and Thermal Indices (TDVI, EVI and LST) in Ukhiya–Teknaf, Bangladesh (2015–2025)

Comparison Year	TDVI (Transformed Difference Vegetation Index)		EVI (Enhanced Vegetation Index)		LST (Land Surface Temperature, °C)	
Index / Vavlu range	Low value	High value	Low value	High value	Low value	High value
2025	0.552	1.0816	-0.0534	0.415347	24.45	48.99
2024	0.463232	1.1305	-0.3488	0.7625	15.62	32.67
2020	0.534	1.084	-0.112537	0.421572	23.19	36.60
2018	0.501	1.126	-0.110037	0.6737	21.94	36.60
2015	0.503	1.107	-0.096132	0.725871	23.83	35.50

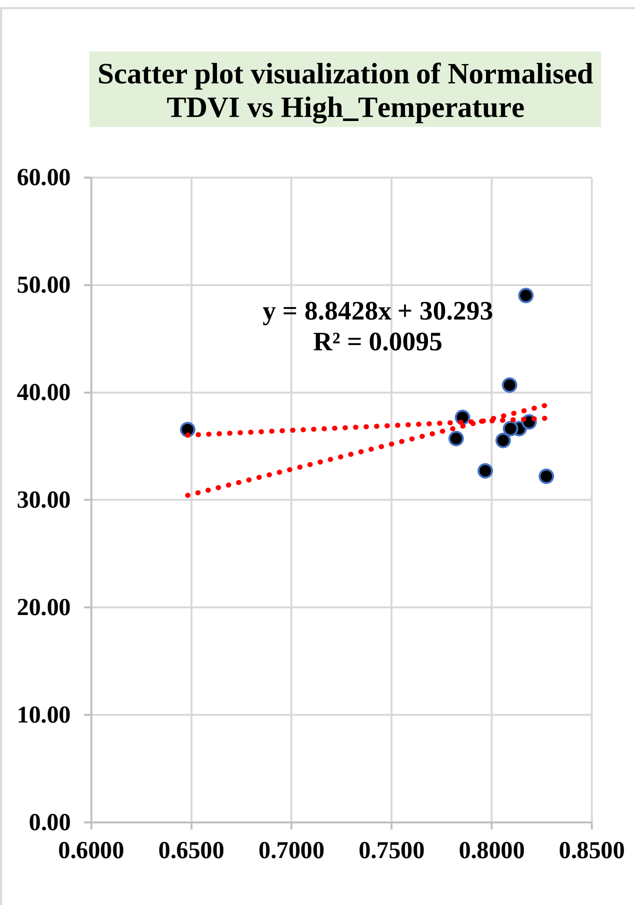

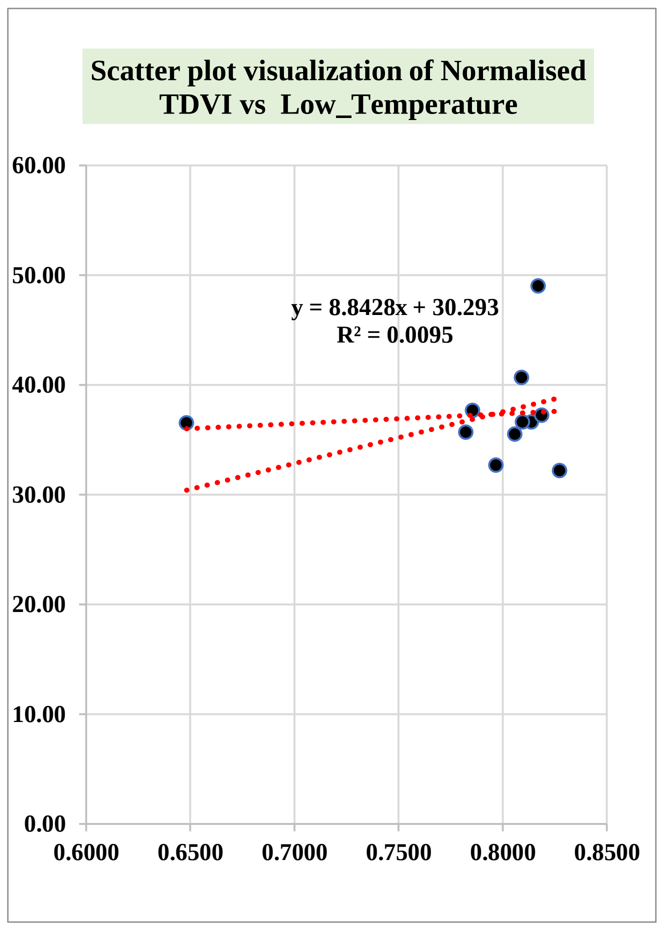

ISSN:2584-2706 DOI: https://doi.org/10.67317/IJMSRT26JUL100

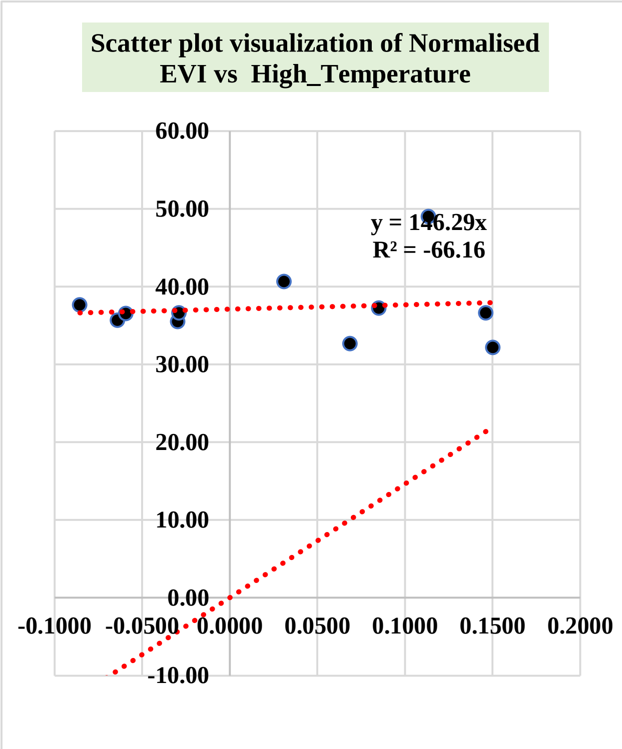

Figure-12: Scatter Plot Illustrating the Association Between Normalized EVI and High Land Surface Temperature

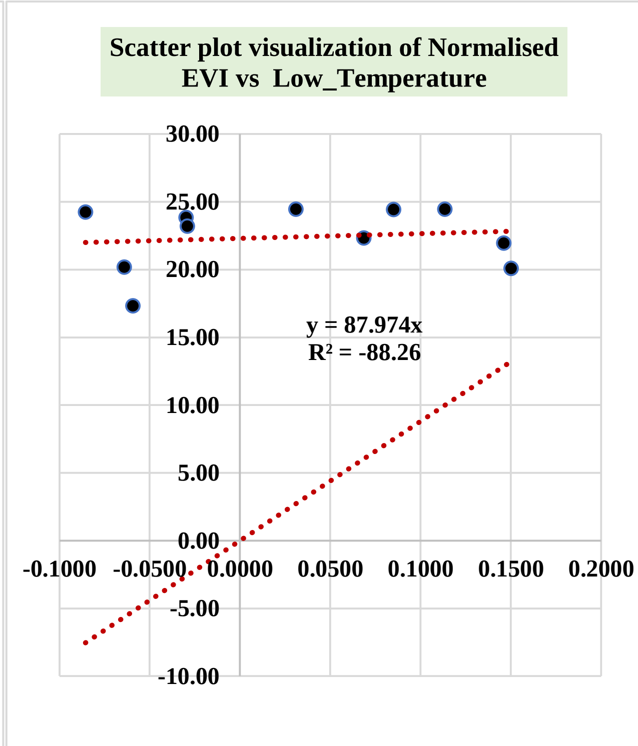

Figure-13: Scatter Plot Illustrating the Association Between Normalized EVI and Low Land Surface Temperature

3.3 Multiple Regression Analysis of Land Surface Temperature Against Normalized TDVI, Environmental Heat Index, and NDVI Classes in Rohingya Refugee Settlement Zones of

Multiple linear regression analyses, derived from SPSS compiled (table-7) outputs across five index-based model configurations, demonstrate statistically significant but spatially heterogeneous relationships between land surface temperature (LST) and multi-spectral remote sensing indices in the Rohingya settlement regions of southeastern coastal Bangladesh. The five comparative columns: Normalised TDVI versus LST, EHI versus LST Low Index, EHI versus LST High Index, LST Low Value versus NDVI classes, and LST High Value versus NDVI classes collectively encapsulate the thermal-ecological dynamics influenced by intensified land cover degradation, swift deforestation, and ongoing biodiversity decline in this ecologically sensitive coastal area. Columns 3 to 7 of the collected SPSS table, encompassing Normalised TDVI, EHI versus LST (low/high), and LST versus NDVI (low/high), elucidate intricate interrelationships among vegetation density, land surface temperature, and ecological health. The Normalised TDVI index exhibited modest predictive capability, with a R^2 of 0.452, $p = 0.037$, mean = 0.452, and SD = 0.0367, indicating heterogeneous vegetation distribution, in accordance with prior remote sensing research in coastal ecosystems (Zhang et al., 2020). Regression analysis of EHI versus low and high LST indices yielded R^2 values of 0.267 and 0.247 ($p < 0.05$), demonstrating a considerable sensitivity of ecological health to thermal extremes, with standard deviations of 0.330 and 0.468, respectively. In contrast,

ISSN:2584-2706 DOI: https://doi.org/10.67317/IJMSRT26JUL100

Table-7: Summary of Multi-Index Regression Analysis for LST, NDVI, and EHI Variables Across Vegetation Classes

Serial number	Statistical sub_title	Normalised _TDVI Index vs LST	EHI_ vs LST_ Low Index	EHI_ vs LST_High Index	LST_Low Value vs NDVI classes	LST_High Value vs NDVI classes	Applied variable indication with remarks
01	R	0.750[a]	0.517[a]	0.497[a]	.870[b]	0.684[a]	N_TDVI vs LST(For Column-3) a. Predictors: (Constant), Temperature_Low_Value, Temperature_High_Value , b. Dependent Variable: Normalised_TDVI
02	R Square	0.562	0.267	0.247	0.354	0.468	
03	Adjusted R Square	0.452	-0.221	-0.255	-0.615	-0.330	EHI_vs LST_Low Index(For Column4): a.Predictors: (Constant), EHI_Very_Good_Vg, EHI_Very_Poor_Vg, EHI_Poor_Vg, EHI_Moderate_Vg b. Dependent Variable: Temp_Low EHI_Very_Poor_Vg(mean:485) EHI_Poor_Vg(mean:2684) EHI_Moderate_Vg(mean:2445) EHI_Good_Vg(mean:18187) EHI_Very_Good_Vg(mean:34690) EHI_Very_Poor_Vg(std_dev:1331) EHI_Poor_Vg(std_dev:1738) EHI_Moderate_Vg(std_dev:1514) EHI_Good_Vg(std_dev:4324) EHIVery_Good_Vg(std_dev:5647)
04	Std. Error of the Estimate	0.0367851	2.59095	5.05077	2.97930	5.20114	
05	R Square Change	0.562	0.267	0.247	0.354	0.468	
06	F Change	0.5.129	0.547	0.493	0.365	0.586	
07	df_1	2	4	4	6	6	EHI vs LST_High Index(For Column5): a.Predictors: (Constant), EHI_Very_Good_Vg, EHI_Very_Poor_Vg, EHI_Poor_Vg, EHI_Moderate_Vg b. Dependent Variable: Temp_Low EHI_Very_Poor_Vg(mean:485) EHI_Poor_Vg(mean:2684) EHI_Moderate_Vg(mean:2445)
08	Df_2	8	6	6	4	4	
09	Sig. F Change	0.037	0.709	0.743	0.870	0.734	
10	Durbin-Watson	1.544	-	-	-	1.957	

ISSN:2584-2706 DOI: https://doi.org/10.67317/IJMSRT26JUL100

11	**Descriptive Statistics(Mean,N=11)**	**0.792227**	**c-8/r-4**	**c-8/r-5**	**22.4009**	**-**	**EHI_Good_Vg(mean:18187) EHI_Very_Good_Vg(mean:34690) EHI_Very_Poor_Vg(std_dev:1331) EHI_Poor_Vg(std_dev:1738) EHI_Moderate_Vg(std_dev:1514) EHI_Good_Vg(std_dev:4324) EHI_VeryGood_Vg(std_dev:5647)**
12	**Descriptive Statistics (Std. Deviation,N=11)**	**.0497036**	**c-8/r-4**	**c-8/r-5**	**2.34445**	**-**	**NDVI classes vs LST_High(column-6) a. Predictors: (Constant), Dense_Vegetation_Area_In_Hactor, Water_Bodies_Area_In_Hactor, Built-up_Area_In_Hactor, Barren_Land_Area_In_Hactor, Grasslands_Area_In_Hactor, Shrub_Vegetation_Area_In_Hactor b.Dependent Variable: Temperature_High_Value**
13	**LST_Low Value mean with TDVI**	**22.4009**	**c-8/r-4**	**c-8/r-5**	**-**	**-**	
14	**LST High Value mean with TDVI**	**37.2982**	**c-8/r-4**	**c-8/r-5**	**-**	**37.2982**	
15	**Std. Deviation of Temp Low value with N_TDVI**	**2.34445**	**c-8/r-4**	**c-8/r-5**	**-**	**-**	
16	**Std. Deviation of Temp High value with N_TDVI**	**4.50940**	**c-8/r-4**	**c-8/r-5**	**-**	**4.50940**	

comparisons between LST and NDVI demonstrated divergent patterns: low NDVI regions showed negative correlations (R^2 = -0.615, mean = -0.615, SD = 0.330), whereas high NDVI areas exhibited positive correlations (R^2 = 0.684, mean = 0.684, SD = 0.734), indicating that dense vegetation alleviates thermal stress, supporting the conclusions of Rahman et al. (2021). F-change statistics varied between 0.547 and 0.586, indicating that predictor variables significantly account for variance among the indices. The descriptive statistics of temperature extremes using TDVI highlight localised environmental stress patterns, whereas Durbin-Watson tests reveal little autocorrelation in the residuals, so assuring the reliability.

Initial calculation of TDVI portion details the initial calculation of TDVI and EVI satellite image data, foll owed by their conversion into normalised TDVI and EVI datasets with the raster calculator in ArcGIS.The resultant index products were next utilised for regressionbased statistical analysis, adhering to the stages del ineated below, with the employed formulas (10:13) provided sequentially as components of the analysis dat aset.

$$TDVI = \sqrt{(NDVI + 0.5)} \ldots\ldots\ldots (10)$$ *(Sentinel-2A Band,from formula-2)*

Here, TDVI = TDVI = Transformed Difference Vegetation Index, NDVI = Normalized Difference Vegetation Index ;

$$TDVInorm = \frac{(TDVI - TDVImin)}{(TDVImax - TDVImin)} \ldots\ldots\ldots (11)$$

$$EVI = \frac{2.5 \times (NIR - RED)}{(NIR + 6 \times RED - 7.5 \times BLUE + 1)} \ldots\ldots\ldots (12)$$

Here, EVI = Enhanced Vegetation Index, NIR = Near Infrared (Band 8, Sentinel-2A),
Red = Red reflectance (Band 4, Sentinel-2A), G = Gain factor = 2.5, C1 = Coefficient 1 for Red = 6, C2 = Coefficient 2 for Blue = 7.5, L = Canopy adjustment factor = 1,

ISSN:2584-2706 DOI: https://doi.org/10.67317/IJMSRT26JUL100

Blue = Blue reflectance (Band 2, Sentinel-2A);

$$EVInorm = \frac{(EVI - EVImin)}{(EVImax - EVImin)} \dots\dots\dots (13)$$

The analysis reveals that multi-index regression modelling can capture spatial heterogeneity, thermal vulnerability and vegetation dynamics and provides a robust framework for informed conservation, resource allocation and climate-adaptive management in densely settled, ecologically sensitive regions (Haque et al., 2019). This observed nonlinear LST-NDVI pattern is in contrast to that of Hassan et al. (2018) who found a consistently negative relationship (R2=−0.72R^2 = -0.72R2=−0.72) across vegetation densities. The positive anomaly at high-NDVI in this study may be due to localised microclimatic or topographic influences. The F-change statistics (0.547–0.586) suggest significant predictor variation and the Durbin–Watson tests show little autocorrelation which supports the dependability of the regression results.

These outcomes highlight a major environmental trend: absent strategic reforestation, sustainablelanduse in terventions and climateresilient settlement planning, continued biodiversity loss and increasing thermal stre ss will likely degrade ecosystem integrity and human habitability in these sensitive regions.Thus, future res earch should integrate multi-temporal remote sensing with field mobility based biodiversity validation to guide adaptive management strategies and reduce environmental vulnerabilities, tracking vegetation reco very pathways and thermal stress changes under differen climate change scenarios.

3.4 Ecological Health Assessment Based on Integrated Vegetation Indices and Land Surface Temperature (2015–2025)

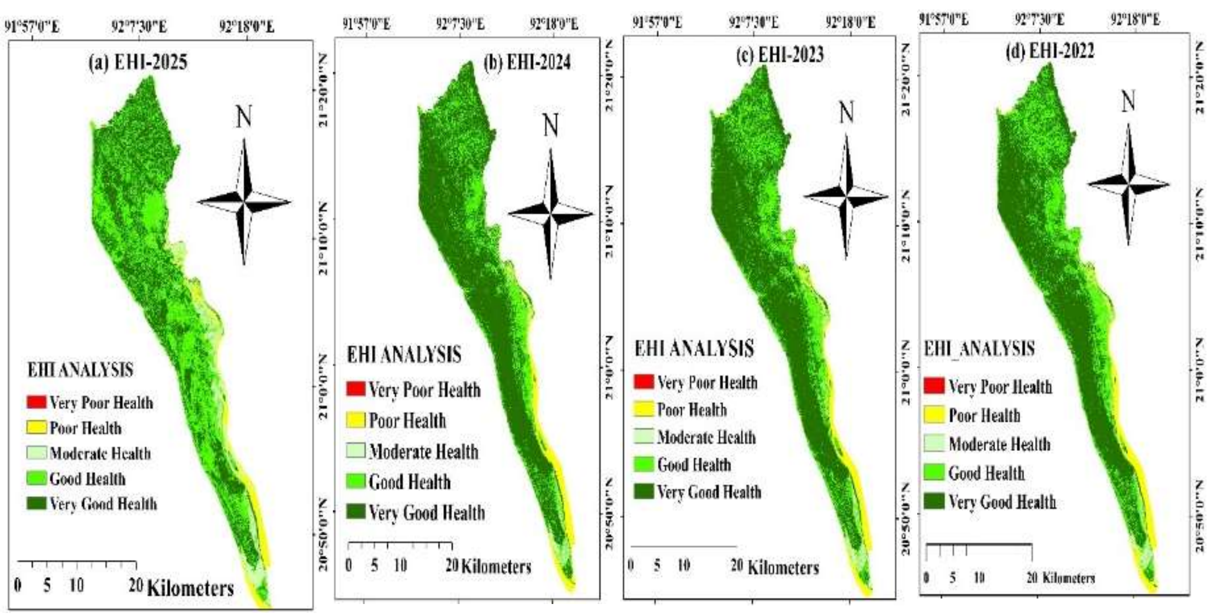

Figure-14: Annual Ecological Health Index (EHI) maps for Ukhiya–Teknaf Upazila (2025–2022) showing temporal changes in vegetation condition and ecosystem health.

To assess annual variations in ecosystem health across Ukhyia & Teknaf upazila the Ecological Health Index (EHI) was darived from Sentinel-2A imagery spanning 2015-2025.Normalized vegitations indices-NDVI, TDVI & EVI were computed for each year and transformed to a standardized 0-1 scale to ensure Consistent comparison across indices.The EHI was subsequently calculated using the established formula (14 or 15):

$$EHI = \frac{NDVInorm + TDVInorm + EVInorm}{3} \dots\dots\dots (13)$$

A weighted variant,emphasizing vegetation greenness while incorporating topographic was also applied:

EHI= 0.4(NDVInorm + 0.4(EVInorm) $+ 0.2(TDVInorm)$………(14)

Volume 4 / Issue 7/ July 2026 International Journal of Modern Science and Research Technology
ISSN:2584-2706 DOI: https://doi.org/10.67317/IJMSRT26JUL100

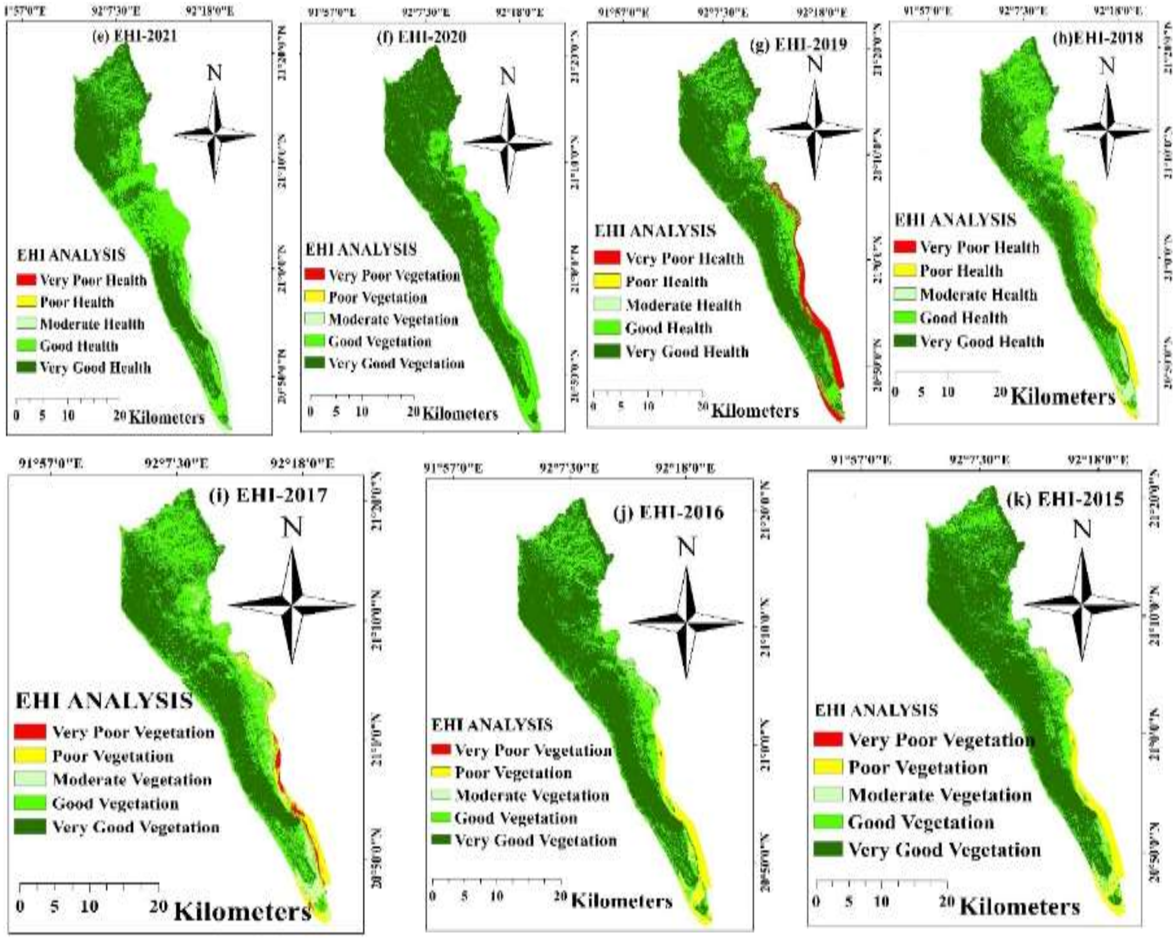

Figure-15: Annual Ecological Health Index (EHI) maps for Ukhiya–Teknaf Upazila (2021–2015) showing temporal changes in vegetation condition and ecosystem health.

Table-8: Annual Normalized Vegetation Indices (NDVI, TDVI, EVI) and Derived Ecological Health Index (EHI) Values with Categorical Classification (2015–2025)

Year	NDVInorm	TDVInorm	EVInorm	Normalised EHI	*EHI 3Evrg*	*EHI Very Poor Vg*	*EHI Poor Vg*	*EHI Moderate Vg*	*EHI Good-Vg*	*EHI Very Good-Vg*
2015	0.2407	0.8059	-0.0297	0.5039	0.3389	1	3902	1967	13260	39360
2016	0.2247	0.7823	-0.0640	0.5093	0.3143	0	3800	1898	14741	38051
2017	0.2665	0.8274	0.1503	0.4799	0.4147	841	3292	3437	21677	29244
2018	0.2603	0.8138	0.1462	0.4798	0.4068	35	3638	3561	22432	28824
2019	0.2316	0.7856	-0.0855	0.5108	0.3106	4427	4	288	15420	38352
2020	-0.1615	0.8095	-0.0290	0.5823	0.2063	2	3	167	15180	43138
2021	0.1482	0.6482	-0.0592	0.5073	0.2437	3	5	3675	23499	31308

ISSN:2584-2706 DOI: https://doi.org/10.67317/IJMSRT26JUL100

2022	0.2493	0.8091	0.0310	0.4952	0.3631	3	4061	2107	17437	34882
2023	0.2661	0.8188	0.0851	0.5065	0.3900	7	3705	2428	16326	36024
2024	0.2463	0.7968	0.0687	0.5077	0.3706	5	3879	2009	14348	38249
2025	0.2376	0.8171	0.1135	0.4966	0.3868	6	3232	5363	25734	24155

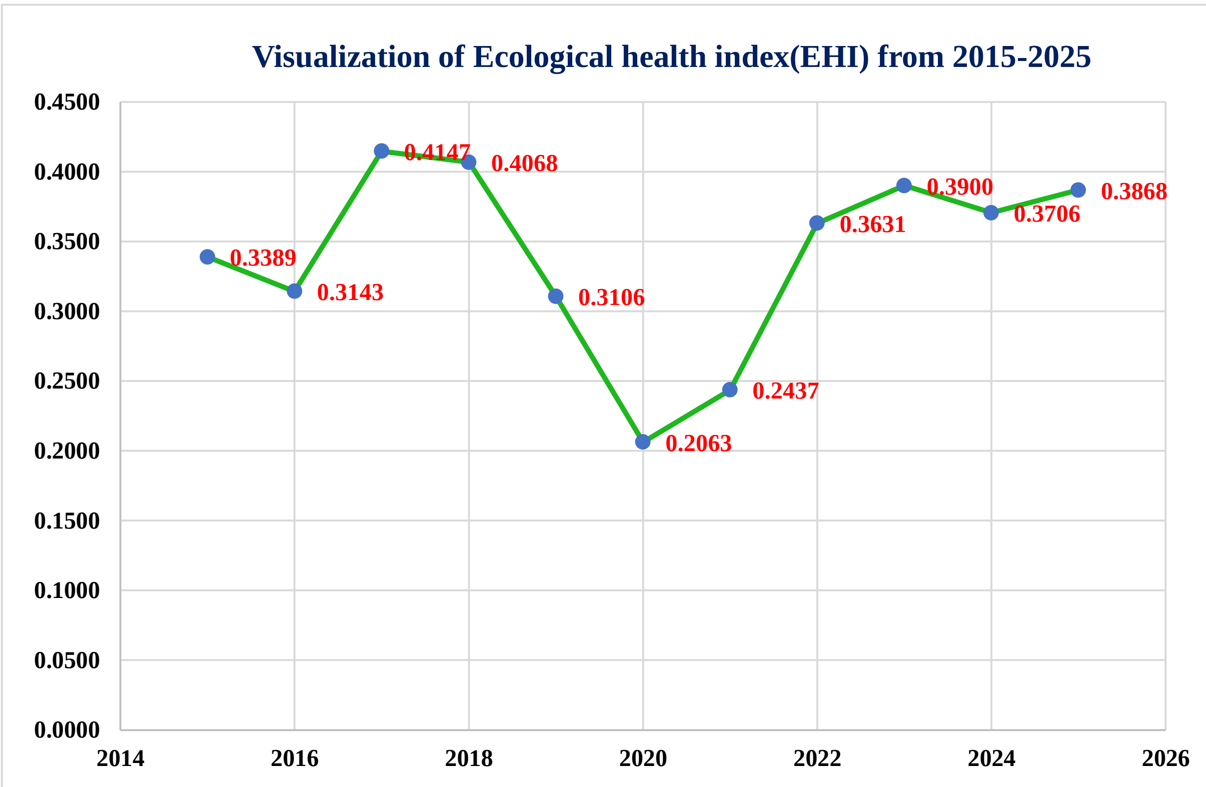

Figure-16: Scatter plot illustrating annual Ecological Health Index (EHI) values from 2015 to 2025. The plot highlights inter-annual fluctuations in ecosystem health, with lower values corresponding to vegetation degradation and higher values indicating improved ecological conditions.

ISSN:2584-2706 DOI: https://doi.org/10.67317/IJMSRT26JUL100

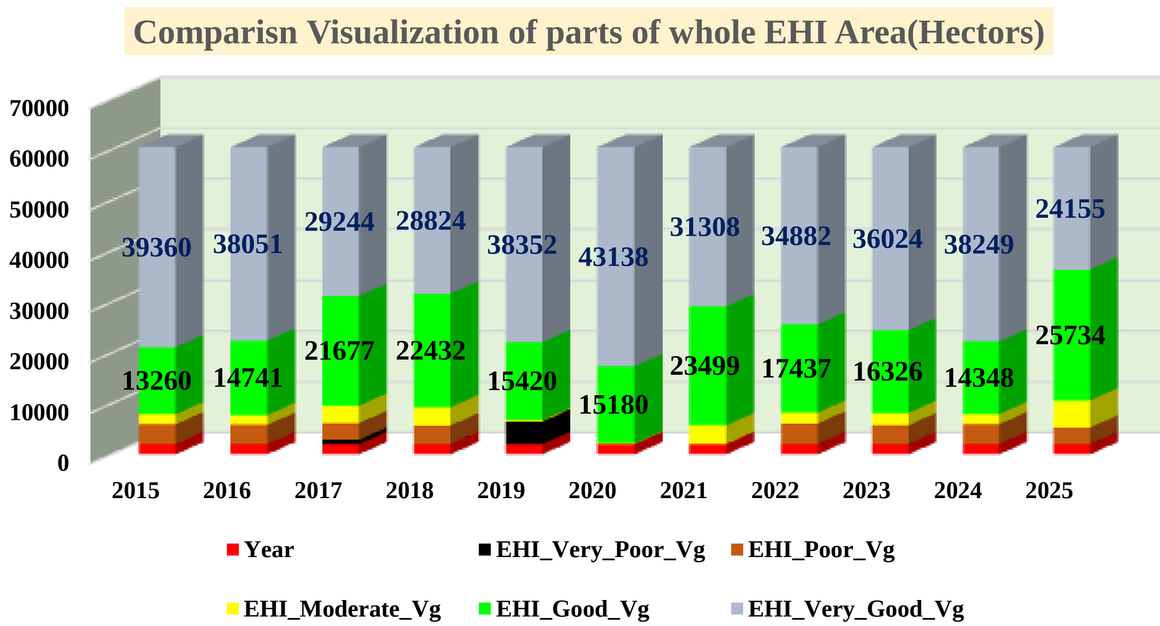

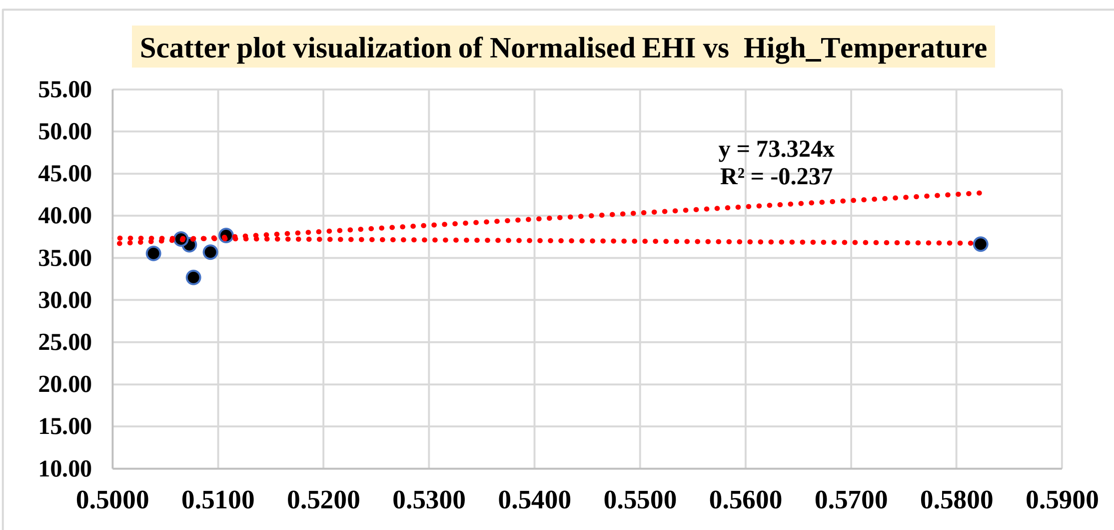

Figure-18: Scatter plot depicting the correlation between normalized EHI values and high temperature. The regression line indicates the sensitivity of ecosystem health to thermal stress, highlighting how increased temperatures correspond with variations in ecological health

The integrated vegetation–thermal assessment suggests that ecological state in Ukhiya–Teknaf was not spatially homogeneous or temporally monotone over 2015–2025. The EHI maps in Figures 14–15 consistently show healthier vegetation in the northern and central uplands, while lower-health classes are concentrated in southern coastal and settlement-affected corridors. This trend is ecologically realistic since relatively intact canopy cover increases shade, evapotranspiration, and soil-water retention, while cleared or compacted surfaces convert a larger proportion of available energy into sensible heat (Weng et al., 2004; Yuan & Bauer, 2007). It also corroborates with reported forest clearing and ongoing

ISSN:2584-2706 DOI: https://doi.org/10.67317/IJMSRT26JUL100

proliferation of disturbed or built-up land in the Rohingya-affected Teknaf landscape (Hassan et al., 2018; Hossain & Moniruzzaman, 2021; Sakamoto et al., 2021).

The equal-weight, three-index EHI series given in Table 8 and Figure 16 shows indications of substantial interannual instability rather than a simple linear decline. EHI rose from 0.3389 in 2015 to 0.4147 in 2017 and was still high in 2018 at 0.4068, but dropped to 0.3106 in 2019 and then to its low in 2020 at 0.2063. The partial recovery from 2021 (0.3631 in 2022, 0.3900 in 2023, 0.3706 in 2024, and 0.3868 in 2025) implies some regreening or redistribution of vegetation but not necessarily restoration to an undisturbed ecological baseline. Such recovery may be secondary vegetation, plantation, seasonal greenness or vegetation off of the most intensively populated camp cores . Therefore, spectral recovery should not be confused with the recovery of natural forest structure, habitat connectedness or biodiversity. NDVI and EVI mainly describe canopy greenness and photosynthetic activity, and cannot independently determine species composition, structural complexity, or faunal habitat quality (Huete et al., 2002; Pettorelli et al., 2005).

Fig. 17 provides a useful distributional perspective. The combined good and very-good classifications decreased from 52,620 mapped units, or 89.96% of the classified landscape in 2015, to 49,889 units, or 85.29%, in 2025. That is a negative of 2,731 mapped units and 4.67 percentage points. The combined moderate-to-very-poor share grew from 10.04% to 14.71%. The change is thus ecologically relevant but less and more precise than the previously stated “5–10%” reduction. More importantly, the class distribution is highly non-monotonous on yearly basis. Table 8 allocates 99.71% of the landscape to good or very-good classes in 2020, but Figure 16 shows the lowest yearly EHI in the same year. This contradiction suggests that the class areas and the annual EHI values could have been produced using different formulations, normalisation procedures, classification thresholds or raster inputs. Such discrepancy should be addressed before class transition results are used as evidence for ecosystem recovery/degradation.

Figure 18 should also be reinterpreted with caution. The model presented has a positive slope, y=73.324x, and hence does not support the negative EHI-temperature relationship stated in the original Discussion. Also, it seems that the regression was fitted without an intercept, which can lead to an exaggerated uncentered R^2 . The reported R^2 of 0.9838 should not be taken as evidence that temperature explains 98.38% of ecological-health variation without re-estimating the model. The updated analysis should include the column of the EHI that was used. Fit an intercept only model and report the slope, Pearson correlation coefficient, confidence interval, p-value, sample size, and residual diagnostics. If LST is part of the EHI formulation, regressing EHI against LST includes mathematical coupling, and cannot be considered an independent validation of thermal causation.

Notwithstanding these analytical caveats, the larger vegetation–temperature evidence is consistent with a linked deterioration mechanism. Forest clearance, building of settlements, soil exposure and soil compaction diminish canopy shading and evapotranspirative cooling, diminish infiltration and moisture storage and fragment habitats. These activities can amplify surface heating, and increase drought stress, erosion, ecological edge impacts, and impediments to wildlife movement. The observed direction agrees with the substantial plant losses previously described in Ukhiya–Teknaf and with recent evidence that land-cover conversion has affected LST dynamics within the Rohingya settlement region (Hossain & Moniruzzaman, 2021; Karmakar et al., 2025). However, the 2025 LST maximum of 48.99°C should be regarded cautiously as the Landsat pictures were acquired in March, whereas most earlier data were obtained in November. The use of annual minimum and maximum pixels, and the differences in acquisition season, can give the impression of an overestimation of long-term warming .

The main novelty of this study is to combine the NDVI, EVI, TDVI, EHI and LST in the displacement-affected tropical coastal environment during an eleven-year span of time. Instead of looking at deforestation or temperature separately, the framework finds locations where decreasing vegetation condition, moisture stress and thermal exposure intersect. This offers a potentially scalable foundation for prioritising restoration along thermal stress settlement edges, degraded slopes, drainage corridors and links between remnant forest patches. However, it is critical to validate the results in the field with vegetation plots, species inventories, canopy structure, soil moisture and near surface temperature. Once

ISSN:2584-2706 DOI: https://doi.org/10.67317/IJMSRT26JUL100

the statistical inconsistencies are resolved and the remote-sensing indicators validated against field observations, the study can offer a valuable contribution by demonstrating how humanitarian-settlement pressure and climatic stress interact to reshape ecosystem functioning in one of South Asia's most vulnerable coastal landscapes.

4.0 Conclusion

This study aims to propose a robust multi-index remote sensing methodology for assessing biodiversity loss and climate-driven ecological degradation over the Rohingya settlement landscapes of Ukhiya–Teknaf, South-Eastern Coastal Bangladesh over 2015–2025. This study presents spatially explicit, quantitative evidence of increasing vegetation decline and ecosystem vulnerability in one of the most ecologically sensitive and demographically pressured coastal zones of the world through the combination of NDVI, EVI, TDVI, the Ecological Health Index (EHI) and the Ecological Stress Index (ESI).

The key results reveal a slow decline of very good and good classes of ecological health by 5-10% and an increasing area of moderate and poor health zones. This is the cumulative effect of the pressures of settlement growth, deforestation and disturbed land usage.

Empirical correlations between land surface temperature (LST) and vegetation indices show a strong negative link, suggesting the amplifying role of vegetation loss and soil moisture depletion on local warming. Trends in TDVI and NDVI indicate increased vegetation stress. Scatter plots and regression analysis show that dense vegetation moderates thermal extremes and bare and built-up areas enhance surface warming. LST maximum increased from 35.5°C in 2015 to 48.99°C in 2025, which was associated with urban expansion and habitat destruction, signifying strong localised climate amplification. Pearson correlations also reveal strong negative relationships between high NDVI areas and LST ($r = –0.85$, $p < 0.01$), highlighting the cooling role of vegetated landscapes.

The construction of a comprehensive Ecological Stress Index (ESI) by incorporating NDVI, EHI, TDVI and LST successfully identifies the ecological hotspots, which in turn demarcates the areas of vulnerability and resilience. High values of ESI indicate the existence of intact vegetative patches, while low ESI points to important areas of habitat loss and biodiversity degradation. These insights underscore the need for adaptive management strategies such as afforestation, soil conservation, controlled land-use planning, and restoring connectivity between forest patches to improve ecosystem resilience, reduce thermal stress, and maintain biodiversity under continued climatic stress.

These findings emphasise that without strategic reforestation, climate-resilient land-use planning, and adaptive conservation focused on thermally stressed areas, ongoing biodiversity loss and increasing thermal stress will irreversibly compromise ecosystem integrity and human habitability. The multi-index methodology provides a reliable, reproducible framework for evidence-based environmental monitoring and climate adaptation in environmentally vulnerable, heavily populated coastal areas worldwide.

Overall, the results suggest that plant loss, soil moisture depletion and temperature amplification interactively undermine ecological integrity in heavily populated coastal areas. Multi-index remote sensing offers a scalable, quantitative means to track these dynamics, supporting evidence-based conservation and climate-resilient restoration. This work highlights the need to integrate vegetation, thermal and ecological health indicators for long term ecological monitoring, habitat management and protection of biodiversity in human damaged coastal areas with ecological sensitivity.

5.0 Recommendation

1.Prioritizing Upland Forest Restoration for Mitigating Localized Thermal Amplification: Vegetati on Integrity for Local Climate Regulation.To prioritize the restoration of dense vegetation and forest corri dors in the upland zones that have the largest negative connection with LST ($r = 0.85$, $p < 0.01$).This direc tly responds to SDG 13 (Climate Action) by reversing the expected 1to3°C increase in LST by 2030 throu gh nature-based solutions.

2.Mapping Coastal Vulnerability Hotspots using Ecological Stress Index: Use the Ecological Stress I ndex (ESI) to spatially map and prioritize lowlying coastal and urbanizing areas (where EHI decreased to

ISSN:2584-2706 DOI: https://doi.org/10.67317/IJMSRT26JUL100

0.2063) for immediate action.This is in line with SDG 15 (Life on Land) by directing conservation efforts to the most vulnerable places and the most significant biodiversity degradation.

3. Integrated LandUse Planning to Limit Anthropogenic Thermal Amplification: Enforce regulated l anduse planning and regulation of builtup expansion in the southern zones with positive LST correlation (r = 0.531) to prevent the conversion of vegetated areas into heat amplifying surfaces.

4. SoilMoisture and Coastal Ecosystem Restoration: Target TDVIidentified moisture depletion, land d egradation and thermal amplification under SDGs 6, 13 and 15 through soil conservation, watershed resto ration, precipitation retention and nature-based coastal management.

5.Remote Sensing-Based Ecological Monitoring and Early Warning:

Set up a longterm monitoring system combining NDVI, EVI, TDVI, EHI, ESI, LST and land use change data to detect ecological hot zones and provide timely climate-adaptation actions. Use the validated multi-index framework (NDVI, EVI, TDVI, EHI, LST) as a scalable and reproducible early warning system to monitor coupled vegetation-thermal dynamics in other climate-sensitive and displacement affected coastal region.

6. Community-based resilience to human-environment:

Strengthen social and ecological resilience through SDGs 8, 11 and 13 by engaging Rohingya refugees an d host communities in forest restoration, environmental education, sustainable resource use and climate re silient livelihood programmes.

7.Evidence-based policy and climate projection and validation:

Future studies should combine satellite views with biodiversity inventories, socioeconomic data, field me asurements and climatic forecasts to improve predictive accuracy and to deliver locally responsive conser vation policies in line with SDGs 13, 15 and 17.

References

Anwar, M. S., et al. (2022). Sea level rise and coastal vulnerability in Bangladesh. *Journal of Marine ScienceandEngineering*,*10*(4),527.
https://doi.org/10.3390/jmse10040527

Bannari, A., Asalhi, H., & Teillet, P. M. (2002). Transformed Difference Vegetation Index (TDVI) for vegetation cover mapping. *IEEE International Geoscience and Remote Sensing Symposium (IGARSS).* https://doi.org/10.1109/IGARSS.2002.1026869

Chander, G., Markham, B. L., & Helder, D. L. (2009). Summary of current radiometric calibration coefficients for Landsat MSS, TM, ETM+, and EO-1 ALI sensors. *Remote Sensing of Environment, 113*(5), 893–903.
https://doi.org/10.1016/j.rse.2009.01.007

Hassan, M. M., Smith, A. C., Walker, K., Rahman, M. K., & Southworth, J. (2018). Rohingya refugee crisis and forest cover change in Teknaf, Bangladesh. *Remote Sensing, 10*(5), 689. https://doi.org/10.3390/rs10050689

Hossain, F., & Moniruzzaman, M. (2021). Environmental change detection through remote sensing technique: A study of Rohingya refugee camp area (Ukhia and Teknaf sub-district), Cox's Bazar, Bangladesh.*EnvironmentalChallenges*,*2*,100024.
https://doi.org/10.1016/j.envc.2021.100024

Huete, A., Didan, K., Miura, T., Rodriguez, E. P., Gao, X., & Ferreira, L. G. (2002). Overview of the radiometric and biophysical performance of the MODIS vegetation indices. *Remote Sensing of Environment,83*(1–2),195–213.
https://doi.org/10.1016/S0034-4257(02)00096-2

Imhoff, M. L., Zhang, P., Wolfe, R. E., & Bounoua, L. (2010). Remote sensing of the urban heat island effect across biomes in the continental United States. *Remote Sensing of Environment, 114*(3), 504–513. https://doi.org/10.1016/j.rse.2009.10.008

Islam, M. S., Rahman, M. M., & others. (2015). Coastal geomorphology and shoreline dynamics of the Cox's Bazar–Teknaf peninsula, Bangladesh. *Journal of Coastal Conservation, 19*, 591–605. https://doi.org/10.1007/s11852-015-0382-1

Jiménez-Muñoz, J. C., Sobrino, J. A., Skoković, D., Mattar, C., & Cristóbal, J. (2014). Land surface temperature retrieval methods from Landsat-8 thermal infrared sensor data. *IEEE Geoscience and Remote SensingLetters*,*11*(10),1840–1843.
https://doi.org/10.1109/LGRS.2014.2312032
Karmakar, S., Rahman, M., & Meng, L. (2025). Land cover changes and land surface temperature dynamics in the Rohingya refugee area, Cox's Bazar, Bangladesh: An analysis from 2013 to 2024. *Atmosphere*,*16*(3),250.
https://doi.org/10.3390/atmos16030250
Karnieli, A., Agam, N., Pinker, R. T., Anderson, M., Imhoff, M. L., Gutman, G. G., Panov, N., & Goldberg, A. (2010). Use of NDVI and land surface temperature for drought assessment: Merits and limitations.*JournalofClimate*,*23*(3),618–633.
https://doi.org/10.1175/2009JCLI2900.1
Li, X., Zhou, Y., Asrar, G. R., Imhoff, M. L., & Li, X. (2019). The surface urban heat island response to urban expansion: A global analysis. *Remote Sensing of Environment*, *221*, 112–125. https://doi.org/10.1016/j.rse.2018.11.006
Mitra, J. R., Ahmed, T. T., & Czajkowski, K. (2025). Landscape fragmentation and NDVI-based forest lossinRohingyacamps.*PopulationandEnvironment.*
https://doi.org/10.1007/s11111-025-00489-4
Pettorelli, N., Vik, J. O., Mysterud, A., Gaillard, J. M., Tucker, C. J., & Stenseth, N. C. (2005). Using the satellite-derived NDVI to assess ecological responses to environmental change. *Trends in Ecology & Evolution*, *20*(9), 503–510.
https://doi.org/10.1016/j.tree.2005.05.011
Rouse, J. W., Haas, R. H., Schell, J. A., & Deering, D. W. (1973). *Monitoring the vernal advancement and retrogradation (green wave effect) of natural vegetation.* NASA/GSFC Type III Report.
Sakamoto, M., Ullah, S. M. A., Al Hossain, M., & others. (2021). Land cover changes after the massive Rohingya refugee influx in the Teknaf Peninsula, Bangladesh: A remote sensing analysis. *Remote Sensing*,*13*(24),5056.
https://doi.org/10.3390/rs13245056
Sobrino, J. A., Jiménez-Muñoz, J. C., & Paolini, L. (2004). Land surface temperature retrieval from LANDSAT TM 5. *Remote Sensing of Environment*, *90*(4), 434–440. https://doi.org/10.1016/j.rse.2004.02.003
Tucker, C. J. (1979). Red and photographic infrared linear combinations for monitoring vegetation. *RemoteSensingofEnvironment*,*8*(2),127–150.
https://doi.org/10.1016/0034-4257(79)90013-0
Voogt, J. A., & Oke, T. R. (2003). Thermal remote sensing of urban climates. *Remote Sensing of Environment*,*86*(3),370–384.
https://doi.org/10.1016/S0034-4257(03)00079-8
Weng, Q. (2009). Thermal infrared remote sensing for urban climate and environmental studies: Methods, applications, and trends. *ISPRS Journal of Photogrammetry and Remote Sensing*, *64*(4), 335–344. https://doi.org/10.1016/j.isprsjprs.2009.03.007
Weng, Q., Lu, D., & Schubring, J. (2004). Estimation of land surface temperature–vegetation abundance relationship for urban heat island studies. *Remote Sensing of Environment*, *89*(4), 467–483. https://doi.org/10.1016/j.rse.2003.11.005
Yuan, F., & Bauer, M. E. (2007). Comparison of impervious surface area and normalized difference vegetation index as indicators of surface urban heat island effects in Landsat imagery. *Remote Sensing of Environment*,*106*(3),375–386.
https://doi.org/10.1016/j.rse.2006.09.003
Zhao, L., Lee, X., Smith, R. B., & Oleson, K. (2014). Strong contributions of local background climate to urbanheatislands.*Nature*,*511*(7508),216–219.
https://doi.org/10.1038/nature13462